Probability distributions of radiocarbon in open compartmental systems

Ingrid Chanca[1,2], Susan Trumbore[1], Kita Macario[2], Carlos A. Sierra[1,3]

[1]Max-Planck-Institut für Biogeochemie, Hans-Knöll-Str. 10, Jena, Germany.

[2]Laboratório de Radiocarbono, Instituto de Física, Universidade Federal Fluminense, Av. Litorânea s/n, Niterói, RJ, Brazil.
[3]Department of Ecology, Swedish University of Agricultural Sciences, Ulls väg 16, Uppsala, Sweden.

Key Points:

- Predicted radiocarbon distributions in open compartments vary according to the year of observation and model structure
- Expected Δ^{14}C values of ecosystem respiration are in accord with empirical Δ^{14}C data
- Probability distributions of radiocarbon in open compartments provide insights into ecosystem dynamics

Corresponding author: Ingrid Chanca, `ichanca@bgc-jena.mpg.de`

Abstract

Radiocarbon (^{14}C) is commonly used as a tracer of the carbon cycle to determine how fast carbon moves between different reservoirs such as plants, soils, rivers or oceans. However such studies mostly emphasize the mean value (as Δ^{14}C) of an unknown probability distribution. We introduce a novel algorithm to compute Δ^{14}C distributions from knowledge of the age distribution of carbon in compartmental systems at equilibrium. Our results demonstrate that the shape of the distributions might differ according to the speed of cycling of ecosystem compartments and their connectivity within the system, and are mostly non-normal. The distributions are also sensitive to the variations of Δ^{14}C in the atmosphere over time, as influenced by the counteracting anthropogenic effects of fossil-fuel emissions (^{14}C-free) and nuclear weapons testing (bomb ^{14}C). Lastly, we discuss insights that such distributions can offer for sampling and design of experiments aiming to capture the precise variability of Δ^{14}C values in ecosystems.

Plain Language Summary

Radiocarbon is a radioactive isotope of carbon prominent in environmental sciences for tracing the dynamics of ecosystems, especially as recent changes in atmospheric radiocarbon allow tracking excess ^{14}C created by weapons testing in the atmosphere on timescales shorter what than can be determined using radioactive decay. For climate changing mitigation, a crucial uncertainty is the time carbon captured through the photosynthesis spends in ecosystems before being released. For this purpose, radiocarbon can be valuable as a biological tracer; however, it is necessary to accurately link the real age of carbon and its radiocarbon age, as they usually differ. Forests and soils systems are open systems, connecting components with intrinsically different cycling timescales, so that the mean age is representing an age distribution that is not normally distributed. Here we developed an algorithm to compute the ^{14}C contents for models consisting of multiple interconnected carbon pools. Our approach, offers more accurate estimations of the mean ^{14}C content of the system and computations of the distribution of ^{14}C within the system at different points in time. From the results we can have more insights into the dynamics of the carbon cycle and how to better design experiments to improve model-observations comparisons.

1 Introduction

Radiocarbon (^{14}C) is a valuable tool for studying dynamical processes in living systems. In particular, radiocarbon produced by nuclear bomb tests in the 1960s has been used in many contexts as a tracer for the dynamics of carbon in different compartments of the global carbon cycle, including the atmosphere, the terrestrial biosphere, and the oceans (Goudriaan, 1992; Jain et al., 1997; Randerson et al., 2002; Naegler et al., 2006; Levin et al., 2010). As a biological tracer, radiocarbon can be used to infer rates of carbon cycling in specific compartments, and to infer transfers among interconnected compartments. Therefore, radiocarbon is used as a diagnostic metric to assess the performance of models of the carbon cycle (Graven et al., 2017), and new datasets are now emerging to incorporate radiocarbon in model benchmarking (Lawrence et al., 2020).

Carbon cycling in biological systems can be represented using a particular class of mathematical models called compartmental systems (Sierra et al., 2018). As carbon enters a system such as the terrestrial biosphere, it is stored and transferred among a network of interconnected compartments such as foliage, wood, roots, soils, and other organisms. Compartmental systems represent the dynamics of carbon as it travels along the network of compartments (Rasmussen et al., 2016; Sierra et al., 2018), and provides information about the time carbon spends in particular compartments and the entire system (Rasmussen et al., 2016; Sierra et al., 2017). Although there seems to be a direct relation between the time carbon spends in a compartmental system and its radiocarbon dynamics, few studies relate both concepts.

An open compartmental system contains inflows and outflows different from zero (Jacquez & Simon, 1993). Timescales in open compartmental systems are usually characterized by the concepts of *age* and *transit time* (Bolin & Rodhe, 1973; Rasmussen et al., 2016; Sierra et al., 2017). In open systems such as the biosphere, the incorporation and release of carbon occurs continuously, but it is possible to define the concept of *age* as the time elapsed since carbon enters the compartmental system until a generic time. The *transit time* can be defined as the time the carbon needs to travel through the entire system, i.e., the time elapsed between carbon entry until its exit.

In order to estimate these time metrics from ^{14}C measurements, a model linking both carbon and radiocarbon dynamics is required. Thompson and Randerson (1999) have used impulse response functions from compartmental models to obtain ages, transit times, and time-dependent radiocarbon dynamics. However, this approach is computationally expensive and can introduce numerical errors if simulations are not long enough to cover the dynamics of slow cycling pools.

Explicit formulas for age and transit time distributions in compartmental systems have been recently developed (Metzler & Sierra, 2017). These formulas do not introduce numerical errors and can describe entire age distributions of carbon for specific pools and for the entire compartmental system. These age distributions suggest that radiocarbon in compartmental systems may consist of a mix of different values, i.e., compartments could be described in terms of radiocarbon distributions that relate the relative proportion of carbon with a particular radiocarbon value. However, until now, radiocarbon is reported and modeled as a single quantity, rather than the mean of an underlying distribution.

Knowledge of the distribution of ^{14}C overlaid on the ^{12}C distribution (C mass) in a compartmental system might give important insights on the model structure that better fits existing data. For example, by comparing the signature of radiocarbon in the pools and their outfluxes, we get insights on the size of the pool model that describes the ecosystem. Conversely, empirical knowledge of the radiocarbon distribution of a particular system, can play a significant role in determining the most appropriate model to describe a system.

Model-data comparisons using radiocarbon are made more complex by the fact that atmospheric ^{14}C is continuously changing. This is particularly important after the 1960s when the nuclear bomb tests liberated large amounts of thermal neutrons to the atmosphere, contributing to the formation of radiocarbon (bomb ^{14}C). In addition, large quantities of fossil-fuel derived carbon (^{14}C-free) have been emitted to the atmosphere, diluting the atmospheric radiocarbon signal and producing a fast decline of radiocarbon values in recent years (Graven et al., 2017). Therefore, we would expect a different radiocarbon distribution for every year in a compartmental system.

Obtaining a simple and accurate method to estimate radiocarbon distributions as a function of the year of observation is, therefore, of great interest for experimental and modeling studies.

The main objective of this manuscript is to introduce a method to obtain distributions of radiocarbon in compartmental systems at steady-state. In particular, we ask the following research questions: (i) How do distributions of radiocarbon change over time as a consequence of changes in atmospheric radiocarbon? (ii) How do empirical data compare to these conceptual radiocarbon distributions? (iii) What insights can these distributions provide for experimental and sampling design for improving model-data comparisons by capturing the entire variability of Δ^{14}C values?

The manuscript is organized as follows: First, we provide the necessary theoretical background to obtain age and transit time distributions from compartmental systems. Second, we describe an algorithm that computes radiocarbon distributions for particular years using an age or a transit time distribution and an atmospheric radiocarbon curve. Third, we present an application of our algorithm to a soil compartmental system addressing the research questions above. Finally, we discuss our results in the context of other applications and potential new insights from our approach.

2 Age and transit time distributions in compartmental systems

2.1 Compartmental systems

Compartmental systems describe the temporal dynamics of matter as it travels through a network of compartments until its final release from the system. A set of compartments is translated mathematically as a set of linear or non-linear ordinary differential equations (ODE), whose solutions are the amount of matter in each compartment at a certain time.

We will consider here linear autonomous compartmental systems, characterized by the mass of carbon at time t in m compartments as the vector $\boldsymbol{x}(t)$. The mass of carbon in the compartments changes over time according to the following expression

$$\frac{d\boldsymbol{x}(t)}{dt} = \dot{\boldsymbol{x}}(t) = \boldsymbol{u} + \mathbf{A}\,\boldsymbol{x}(t), \qquad \boldsymbol{x}(t=0) = \boldsymbol{x_0}, \tag{1}$$

where the vector $\boldsymbol{u}$ represents the inputs of carbon into the system, and the $m \times m$ compartmental matrix $\mathbf{A}$ contains in its diagonal entries the cycling rates of the compartments, while the off-diagonal entries consist of the transfer rates among them. In particular, the compartmental matrix in most ecosystem carbon models has an internal structure reflecting transfers between the components (coefficients $\alpha_{i,j}$, representing the proportion of C transferred from compartment j to compartment i) and cycling rates k_i reflecting assumptions of first-order kinetics of loss (at rate $C_i k_i$) from any given compartment:

$$\mathbf{A}_{m,m} = \begin{pmatrix} -k_1 & \alpha_{1,2}k_2 & \cdots & \alpha_{m,m}k_m \\ \alpha_{2,1}k_1 & -k_2 & \cdots & \alpha_{2,m}k_m \\ \vdots & \vdots & \ddots & \vdots \\ \alpha_{m,1}k_1 & \alpha_{m,2}k_2 & \cdots & -k_m \end{pmatrix}, \tag{2}$$

This matrix contains information on the dynamics, structure, and size of a compartmental model. The rate of exit of carbon from the system can also be obtained from this matrix by summing all column elements; i.e., the outputs from a pool that are not transferred to other pools are assumed to leave the compartmental system.

The information of the amount of carbon entering the system to be partitioned among the compartments is contained in the input vector

$$\boldsymbol{u} = \begin{pmatrix} u_1 \\ u_2 \\ \vdots \\ u_m \end{pmatrix}. \tag{3}$$

Linear autonomous systems of the form of equation (1) have an equilibrium point or steady-state solution $\boldsymbol{x}^*$ given by

$$\boldsymbol{x}^* = -\mathbf{A}^{-1}\,\boldsymbol{u}, \tag{4}$$

where the mass of the compartments do not change over time, and inputs are equal to outputs for all compartments.

2.2 Age distributions

We define age τ in a compartmental system as the time elapsed between the time of carbon entry until some generic time (Sierra et al., 2017). For a time-independent system in steady state, a probability distribution of ages of carbon in the compartments can be obtained using stochastic methods. According to Metzler and Sierra (2017), the vector of age densities for the compartments can be obtained as

$$\boldsymbol{f_a}(\tau) = (\mathbf{X}^*)^{-1} \cdot e^{\tau\,\mathbf{A}} \cdot \boldsymbol{u} \tag{5}$$

where $\mathbf{X}^* = \mathrm{diag}\,(x_1^*, x_2^*, \ldots, x_m^*)$ is the diagonal matrix with the steady-state vector of carbon stocks as components, and $e^{\tau\,\mathbf{A}}$ is the matrix exponential.

For the whole system, the age distribution is given by

$$f_A(\tau) = -\mathbf{1}^\intercal \cdot \mathbf{A} \cdot e^{\tau \mathbf{A}} \cdot \frac{\boldsymbol{x^*}}{\|\boldsymbol{x^*}\|}, \tag{6}$$

where the symbol $\|\cdot\|$ represents the sum of the masses in a vector.

2.3 Transit Time distributions

We define transit time as the time elapsed since carbon enters the compartmental system until it leaves the boundaries of the system (Sierra et al., 2017). The transit time is equivalent, therefore, to the age of the outflux. Metzler and Sierra (2017) also provide an explicit formula to obtain the transit time density distribution for a time-independent system at steady state as

$$f_T(\tau) = -\mathbf{1}^\intercal \cdot \mathbf{A} \cdot e^{\tau \mathbf{A}} \cdot \frac{\boldsymbol{u}}{\|\boldsymbol{u}\|}. \tag{7}$$

These distributions are densities, so they integrate to 1

$$\int_0^\infty f_A(\tau)\,d\tau = \int_0^\infty f_T(\tau)\,d\tau = 1. \tag{8}$$

3 Methods

3.1 Radiocarbon distributions from age and transit time distributions

We developed an algorithm to convert age and transit time distributions into Δ^{14}C distributions for any given year of observation.

The algorithm works in three main steps, 1) homogenization, 2) discretization, and 3) aggregation (Figure 1). We describe these three steps in detail in the sections below, using mathematical notation for the system age distribution, but computations are similar for the transit time distribution, and the age distribution of individual compartments.

3.1.1 Homogenization of input data

The main inputs for the algorithm are an age distribution $f_A(\tau)$, and an atmospheric radiocarbon curve $F_a(t)$ that provides the Δ^{14}C value of atmospheric CO_2 for a calendar year t. To homogenize the time scales of both $f_A(\tau)$ and $F_a(t)$, we define the year of observation t_0, as the year of interest to produce the radiocarbon distribution.

Since we are interested in determining the radiocarbon values of material observed in the system at time t_0, we will look in the radiocarbon curve $-t$ years in the past to obtain the radiocarbon values in the system with an age τ. Therefore, atmospheric radiocarbon can be expressed as a function of age, i.e., $F_a(t_0 - t) = F_a(\tau)$ (Figure 1). Now, both the system age distribution $f_A(\tau)$ and the atmospheric radiocarbon curve $F_a(\tau)$ are functions of the continuous variable τ that represents age.

Several atmospheric radiocarbon datasets can be found in the literature (Reimer et al., 2013, 2020; Hogg et al., 2013, 2020; Hua et al., 2013; Levin et al., 1980; Levin & Kromer, 1997; Levin et al., 2010; Graven et al., 2017). Also forecasts of radiocarbon content in the atmosphere can be found in the recent literature (Graven, 2015; Sierra, 2018). However, these atmospheric radiocarbon datasets do not necessarily have the same resolution in time. Some of them provide predictions or data at an annual or four-monthly time step, while in other datasets, some ranges are spaced by decades. To homogenize the resolution of the Δ^{14}C and to transform these radiocarbon datasets into a continuous function of τ, we use a cubic spline interpolation to obtain Δ^{14}C values for any value of τ. After this step, $f_A(\tau)$ can be computed for any value of $\tau \in [0, \infty)$, and $F_a(\tau)$ until the last available date in the chosen radiocarbon atmospheric dataset.

3.1.2 Discretization

Although we have now the age distribution and the radiocarbon data as continuous functions of age, we need to discretize these functions in intervals of size h. The reason for this discretization is that the probability density function of age $f_A(\tau)$ is a measure of the relative likelihood of an infinitesimal amount of mass having an age τ. But ultimately, we are interested in the probability that a small mass has certain radiocarbon distribution. Therefore, we need to discretize the probability density function to a probability mass function along a discrete variable $T \in [0, T_{\max}]$. The new discrete probability function of ages can be defined as

$$P_A(\tau \leq T \leq \tau + h) = \int_{\tau}^{\tau+h} f_A(\tau) d\tau. \tag{9}$$

From this probability function, we can compute the proportion of total mass in the system with an age T as

$$M(T) = \|\boldsymbol{x}^*\| \cdot P_A(T), \tag{10}$$

where

$$\begin{aligned} \sum_{0}^{T_{\max}} P_A(T) &\approx 1, \\ \sum_{0}^{T_{\max}} M(T) &\approx \|\boldsymbol{x}^*\|. \end{aligned} \tag{11}$$

Equation (11) implies that there is an approximation error by discretizing the continuous density function to a finite set of discrete intervals. This approximation error can be minimized by decreasing the size of the intervals h and extending $T_{\max}$ as far as possible.

Once we discretize $f_A(\tau)$ to $P_A(T)$ and obtain discrete proportions of mass with certain age $M(T)$, we proceed to discretize the atmospheric radiocarbon curve with respect to the same discrete interval of ages $T \in [0, T_{\max}]$. This is simply done by computing $F_a(\tau = T)$, which makes the assumption that within each interval $[\tau, \tau + h]$, the atmospheric radiocarbon value is equal to $F_a(\tau)$.

3.1.3 Aggregation

Now we are ready to combine the distribution of mass in the system at discrete age intervals with the atmospheric radiocarbon curve. To do so, we first find for each value of $T \in [0, T_{\max}]$ the corresponding values of mass $M(T)$ and radiocarbon $F_a(T)$. Then, we sum all the masses with similar Δ^{14}C values. The result can be organized as the amount of mass in discrete intervals of Δ^{14}C; i.e., $M(\Delta^{14}\text{C}) = M(F_a(T))$.

These steps can also be visualized through the graphs in Figure 1.

We implemented these three steps in the R programming language, and use the package SoilR (Sierra, Müller, et al., 2012) to obtain the age distribution of the pools, the whole system, and the output flux (equivalent to the transit time) based on equations (5), (6), and (7). The versions used here were R version 4.0.3 and SoilR version 1.1 (Sierra et al., 2014).

Since atmospheric ^{14}C concentration for the past 55,000 years is principally known from the radiocarbon curves, we could easily convert age into atmospheric Δ^{14}C. By matching the Δ^{14}C-based-on-age values with the previously estimated densities, we built barplots, gaining insight into the radiocarbon distributions for the model studied in this work. In the algorithm we defined four functions: *PoolRDC*, *SystemRDC*, *TTRDC*, and *C14hist*. The first three functions take the densities outputs, i.e., the carbon contents discretized by age, from built-in SoilR functions, such as *transitTime* and *systemAge*. The densities are subset to build bins through the *C14hist* function. The logical statements used to construct the bins are based on the atmospheric Δ^{14}C data and according to user-defined bin size b. This structure allows one to plot histogram-like graphs, where the height of the bars represent the amount of mass with corresponding Δ^{14}C values. Thus, our algorithm initialize from a compartmental matrix, an input vector and a radiocarbon calibration curve, and returns an object containing masses of C and their matching decay-corrected Δ^{14}C values, estimated for any given observation year . The match is done by assuming the year of observation as equivalent to the age of the pool or the system equals zero ($t_0 - t = \tau = 0$). This means that past years, or older pool or system ages, are equivalent to the Δ^{14}C signal of the atmosphere of those years corrected by the radioactive decay of ^{14}C (average lifetime of 8,267 years, i.e., half-life of 5,730 years).

Besides the radiocarbon distributions for pools, whole system and output flux, one can also compute the expected value of Δ^{14}C from these distributions in any given observation year. This is done by computing the mean of Δ^{14}C weighted by the amount of carbon in Δ^{14}C bins of size b. The standard deviation of the distribution is obtained as the square root of the difference between the square of the expected value and the expected value of the squares of Δ^{14}C values.

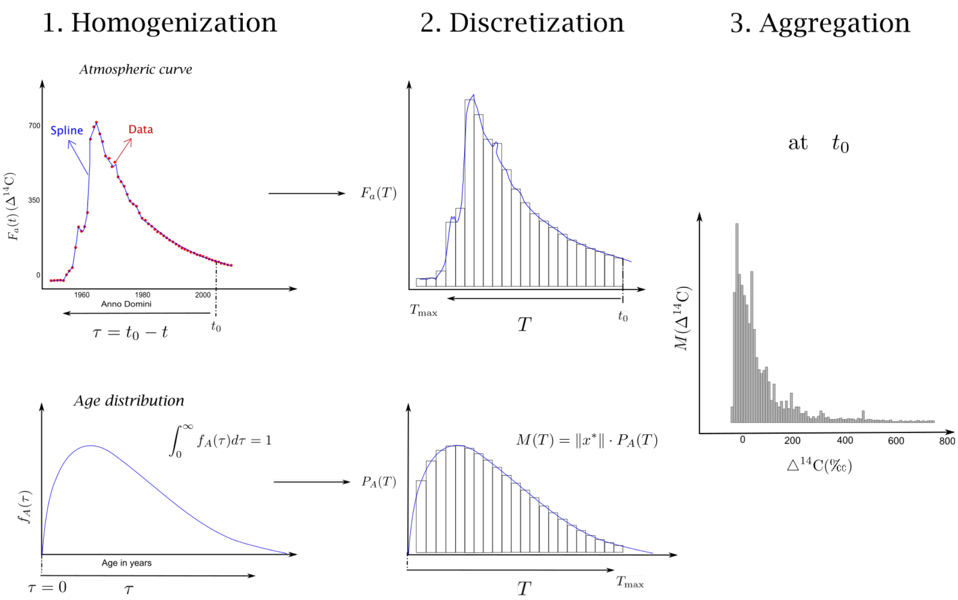

Figure 1. Graphical visualization of the three main steps for the computation of radiocarbon distributions in a compartmental system using an atmospheric radiocarbon curve of the carbon inputs to the systems, and the age distribution of carbon in a compartmental system. Details about each step are provided in the main text.

3.2 Carbon Cycle models

Our approach can be used to obtain radiocarbon distributions for linear compartmental models of any size representing carbon cycling processes at different scales and for different biological systems.

We will focus here on a model that represents the dynamics of soil organic carbon at a temperate forest, which we call therein the Harvard Forest Soil (HFS) model. The model is based on measurements conducted at the Harvard Forest in Massachusetts, USA (Gaudinski et al., 2000; Sierra, Trumbore, et al., 2012). Soil samples collected in O-horizon, corresponding to $0 - 8$ cm depth, and A-horizon ($8 - 15$ cm depth) were fractionated into seven soil fractions called: Dead Roots, Oi, Oe/a L, Oe/a H, A, LF (> 80 μm), A, LF (< 80 μm), and Mineral Associated. They were obtained as follows: The O-horizon was subdivided after hand-picking into leaf litter (*Oi* fraction), recognizable root litter (*Oe/a L* fraction) and humified, i.e., organic matter that has been transformed by microbial action, corresponding to the fraction *Oe/a H*. Samples from the A-horizon were fractionated by density into low-density and high-density portions. The high-density portion corresponds to the *Mineral Associated* fraction. The low-density portion is further subdivided by sieving into recognizable leaf larger than 80 μm (*A, LF (> 80 μm)* fraction) and smaller than 80 μm (*A, LF (< 80 μm)* fraction). Details about the methods employed to fractionate the samples can be found in Gaudinski et al. (2000).

The compartmental model consists of seven pools (Figure 2); one pool corresponds to dead roots x_1, and three pools correspond to three different types of organic matter in the surface layer (O) called Oi, Oe/a L, and Oe/a H, which corresponds to pools x_2, x_3, and x_4 in the model. Two additional pools, called A, LF ($> 80\mu$m), representing material from the A horizon that floats in a dense (1 g cm^{-3}) liquid and does not pass through an 80 μm sieve and A, LF (< 80 μm) (low density fraction passing the sieve), represent the dynamics of two fractions in the soil A horizon with different granulometry, x_5 and x_6, respectively. The seventh pool x_7 represents the dynamics of the mineral associated fraction (Sierra, Trumbore, et al., 2012).

The HFS model was built by fitting of empirical radiocarbon data from the above described samples. Details about the use of the data to build the compartmental model are presented in Sierra, Trumbore, et al. (2012). For the same sites, there are independent data (i.e., data not used for estimating the compartmental matrix) available. The independent data used in this work consists of Δ^{14}C measurements on total soil CO_2 efflux collected in the years 1996, 1998, 2002, and 2008. The number of samples measured corresponding to the respective years was n = 12, n = 28, n = 23, and n = 10 . We used these data to compare the representativity of the mean Δ^{14}C measurements to the expected Δ^{14}C values obtained through our algorithm.

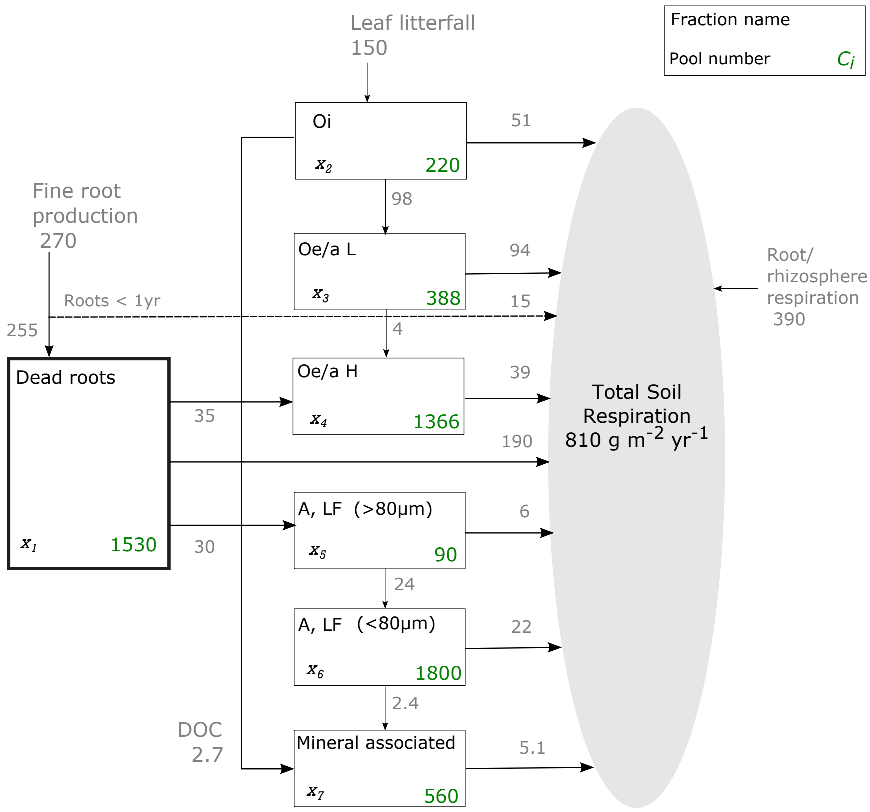

Figure 2. Scheme of HFS model stocks (C_i) and fluxes among compartments (adapted from Sierra, Trumbore, et al. (2012)).

The system of ODE for the HFS model can then be expressed in compartmental form as

$$\begin{pmatrix} \dot{x}_1 \\ \dot{x}_2 \\ \dot{x}_3 \\ \dot{x}_4 \\ \dot{x}_5 \\ \dot{x}_6 \\ \dot{x}_7 \end{pmatrix} = \begin{pmatrix} 255 \\ 150 \\ 0 \\ 0 \\ 0 \\ 0 \\ 0 \end{pmatrix} + \begin{pmatrix} -255/1530 & 0 & 0 & 0 & 0 & 0 & 0 \\ 0 & -150/220 & 0 & 0 & 0 & 0 & 0 \\ 0 & 98/152 & -98/388 & 0 & 0 & 0 & 0 \\ 35/255 & 0 & 4/98 & -39/1366 & 0 & 0 & 0 \\ 30/255 & 0 & 0 & 0 & -30/90 & 0 & 0 \\ 0 & 0 & 0 & 0 & 24/30 & -24/1800 & 0 \\ 0 & 3/152 & 0 & 0 & 0 & 3/25 & -5/560 \end{pmatrix} \begin{pmatrix} x_1 \\ x_2 \\ x_3 \\ x_4 \\ x_5 \\ x_6 \\ x_7 \end{pmatrix}. \tag{12}$$

3.3 Set of parameters

As described before, in order to estimate the radiocarbon distributions and expected values of Δ^{14}C, the algorithm needs the following arguments: a compartmental matrix $\mathbf{A}$, containing the decomposition and transfer rates within the pools; an input vector $\boldsymbol{u}$ containing the input mass to be partitioned among the compartments; the year of observation (equivalent to year of *sampling* in an experimental framework); the number of years in the past one aims to compute the distributions for; and a set of radiocarbon values in the atmosphere, comprising the year of observation and the number of years chosen. An additional argument is h, the discretization size described above, which has a default value of 0.1 years, but could be modified according to user preferences.

For the HFS model, $\mathbf{A}$ is the matrix in equation (12), with the form of equation (2), and $\boldsymbol{u}$ is the numeric vector in the same equation, with similar form as equation (3). We estimated the radiocarbon distributions for different years of observation, in order to address different research questions raised in this work. In the results we present the distributions for the individual pools, total outflux and whole system, for the years: 1965, 2027 and 2100. Additionally, in the *Supplementary Material* we provide the non-stacked radiocarbon distributions of individual pools, total outflux and whole system for the years 1950, 1965, 2027, and 2100. Radiocarbon distributions of the *outflux* are presented for the years: 1996, 1998, 2002, and 2008, as for those years we also have independent Δ^{14}C data from soil CO_2 efflux to compare to our estimations. For all those estimations, the number of years of computation was 1,000 years. The bin size b ([‰]) for plotting the histograms was set as 10 for most of the radiocarbon distributions, except for the year 1965, where it was set up to 40.

3.3.1 Radiocarbon datasets

The radiocarbon values used for years in the past, e.g., AD 1965, were obtained by merging the recently released IntCal20 calibration curve (Reimer et al., 2020), which combines radiocarbon data and Bayesian statistical interpolation for the range 55,000 – 0 cal BP (BP = *before present* = AD 1950), and the records of atmospheric radiocarbon data compiled by Graven et al. (2017), from 1950 to 2015. Graven et al. (2017) also provides radiocarbon data in one-year resolution on the range 1850 to 1949. However, since in this range the estimations were partially based on the previous Northern Hemisphere calibration curve (IntCal13, Reimer et al. (2013)), we decided to subset Graven et al. (2017)'s dataset starting in AD 1950.

For the years in the future, such as AD 2027 and 2100, we made use of the forecast simulations computed by Graven (2015), who simulated Δ^{14}C values in the atmosphere for four Represent Concentration Pathways of fossil fuel emissions: RCP2.6, RCP4.5, RCP6 and RCP8.5. In this work we use the predictions based on the high emissions scenario (RCP8.5), starting in AD 2016.

The Δ^{14}C values in all datasets used in this work are written as the deviation from the standard representing the pre-industrial atmospheric ^{14}C concentration. The raw published values are already corrected for fractionation and decay with respect to the standard. It is equivalent to Δ in Stuiver and Polach (1977). Thus, the equation it follows is

$$\Delta^{14}C = \left[F^{14}Ce^{\lambda_C(1950-y)} - 1\right] \times 1000\,[‰] \tag{13}$$

where $F^{14}C$ is the Fraction Modern (A_{SN}/A_{ON}), i.e., the sample ratio normalised to δ^{13}C by oxalic acid standard (OXII), λ_C is the updated ^{14}C decay constant (equals 1/8267 [y^{-1}]), and y is the year of measurement.

4 Results

4.1 Shape of the radiocarbon distributions and their change over time

Overall, our results show that even though the age and transit time distributions for this compartmental system are static (Figure 3), the radiocarbon distributions are highly dynamic. They change dramatically over time as the atmospheric CO_2 source is affected by the bomb spike and the Suess effect (Suess, 1955), i.e., the effect of the dilution of radiocarbon in the atmosphere due to the emission of fossil fuels (^{14}C-free). Pools that cycle fast, i.e., pools with sharp age distributions peaks, such as *Dead Roots* and *Oi*, followed most closely the radiocarbon dynamics in the atmosphere, while pools that cycle slowly showed a wide range of values. Consequently, the expected Δ^{14}C values also vary largely.

The distributions we obtained for the compartments of the HFS model show very different shapes for the different compartments (Figures 4, 5, and 6, and Figures S2, S3, S4 and S5 in Supplementary Material). In 1965, just after the peak of bomb ^{14}C in the atmosphere due to nuclear weapons tests, pools that cycle fast had a wide Δ^{14}C range with high probability, due to the incorporation of radiocarbon values that changed rapidly over the period AD 1950 – 1965. Compartments that cycle slowly have a narrower distribution with their modes corresponding to negative Δ^{14}C values, as they represent pre-bomb atmospheric signals that varied less.

For the whole system in AD 1965 (Figure 7), the distribution of radiocarbon aggregates the contributions of the different pools, which results in different peaks in the overall distribution. The mode (i.e., the Δ^{14}C with highest mass density) is below 0 ‰ because a large portion of the total amount of carbon is contributed by the mineral associated pool that is predominantly still pre-bomb carbon with little contribution from carbon fixed after 1964. In addition, other pools that cycle fast, contribute relatively small amounts of bomb ^{14}C to the overall distribution.

The radiocarbon distribution in the output flux in AD 1965 (Figure 7), i.e., the radiocarbon distribution that corresponds to the transit time distribution for this year, has three distinct peaks in the distribution. This distribution is very similar to that of the *Dead Roots* pool (Figure S3), which is the main contributor to the total respiration flux. However, other pools also contribute to the respiration flux with their radiocarbon signatures and emphasize fluxes from the fastest cycling pool (Oi) and respiration of carbon that was present in other pools before the bomb peak.

The shapes of the distributions change dramatically for subsequent years after the bomb spike (Figure 5). For AD 2027, the expected Δ^{14}C values of fast pools drop considerably, in parallel with atmospheric ^{14}C, compared to AD 1965. These fast pools do not stored much radiocarbon from the bomb period, and their radiocarbon signatures reflect recent carbon from the atmosphere. In contrast, slow cycling pools in AD 2027 had relatively high Δ^{14}C values, mostly because they still contain radiocarbon from the bomb period. In the output flux, as expected, since the respiration flux is dominated by the faster-cycling pools such as *Dead Roots* and *Oi*, most of the radiocarbon is narrowly distributed around the recent atmospheric Δ^{14}C value in 2027, with almost no contributions from bomb ^{14}C.

By the year 2100, the atmospheric Δ^{14}C values have dropped to -254.5 ‰ (Graven, 2015), reflecting the Suess effect. The distributions of most pools are less variable. Faster cycling pools have dropped to reflect negative Δ^{14}C in the atmosphere over the 73 years since 2027, while the slow pools (*Mineral Associated, A, LF (<* $80\ \mu m$*)* and *Oe/a H* pools) still show a wide range of Δ^{14}C values that includes C fixed during the bomb period (now ∼150 years previously).

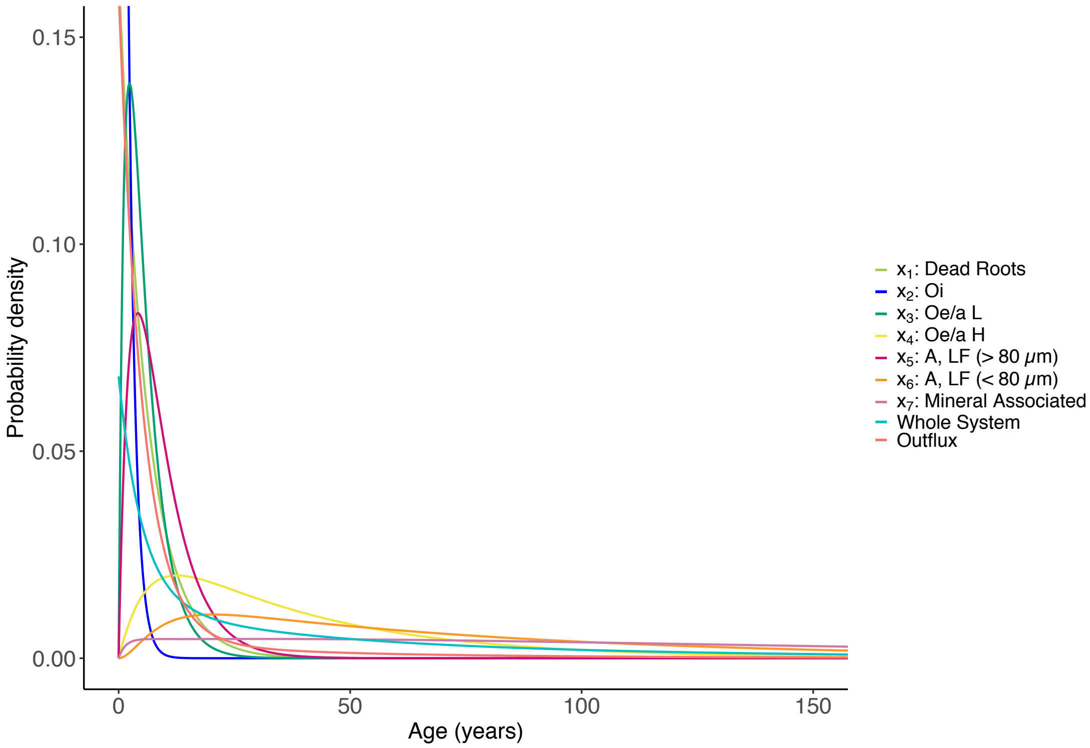

Figure 3. Age distributions for the Harvard Forest Soil model computed in a span of 1,000 years with a resolution of 0.1 year. The x-axis is limited to 150 years and the y-axis is limited to 0.15 for better visualization of the data.

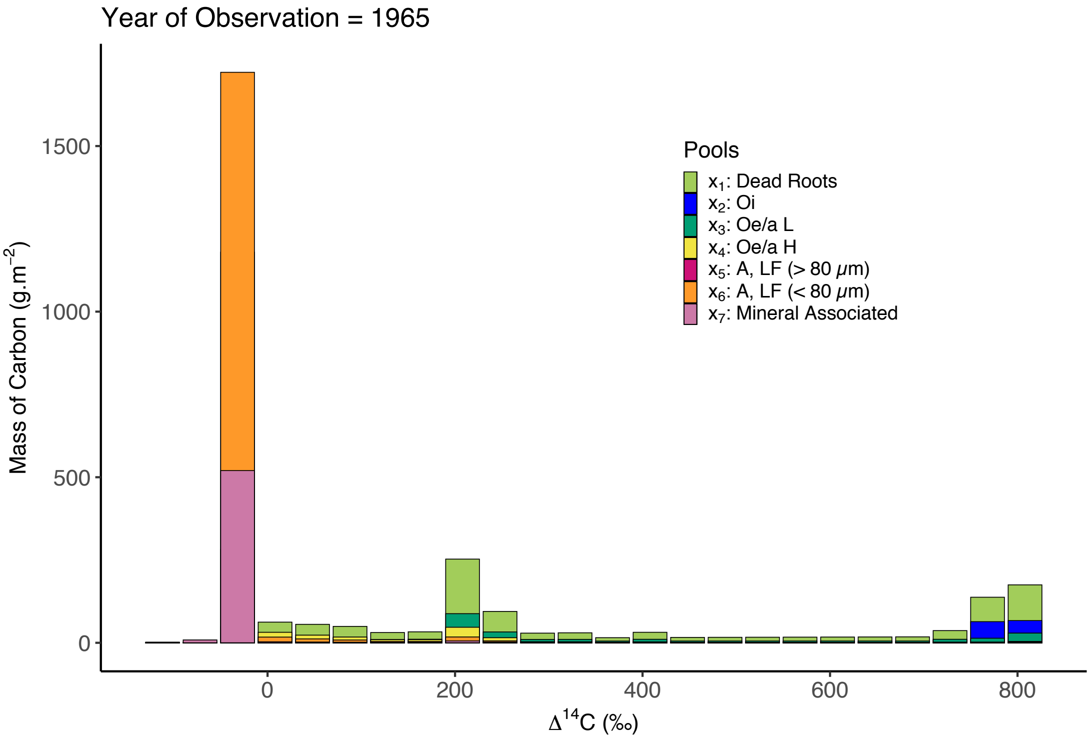

Figure 4. Δ^{14}C distributions of each of the seven pools of the HFS model through the algorithm described above. The year of observation is 1965 – just after the bomb peak in 1964 – and the distributions are computed over 1,000 years. The bin size b is equal to 40 ‰. The expected value and standard deviation of this distribution is 141 ± 280.

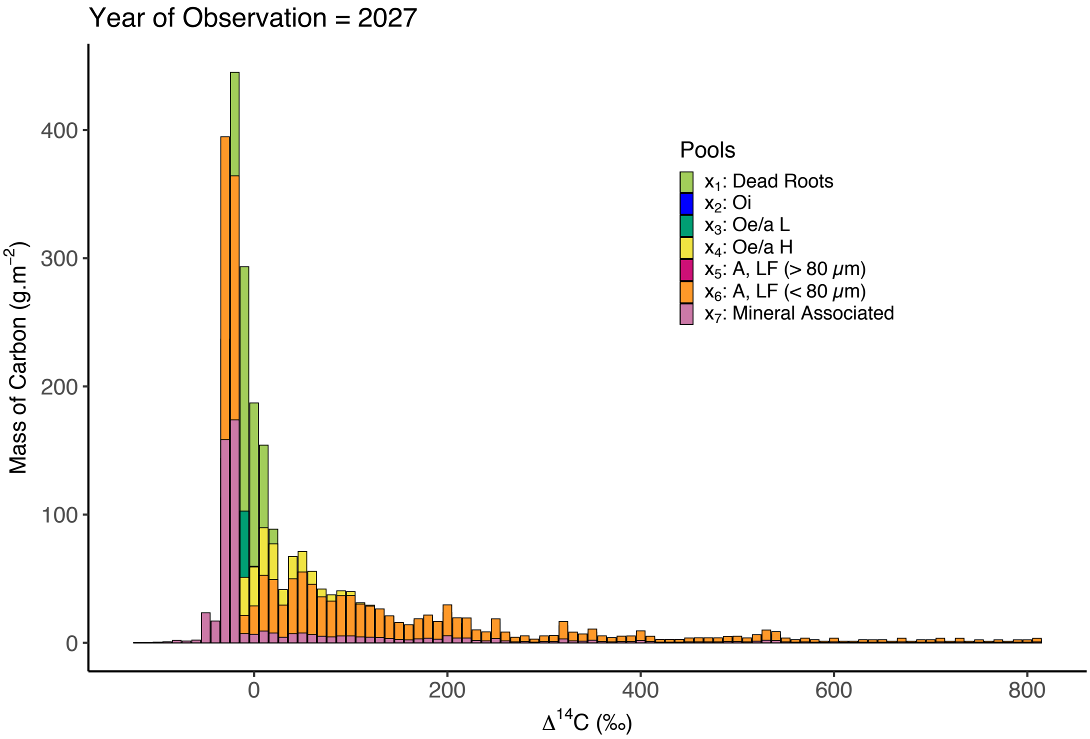

Figure 5. Δ^{14}C distributions of each of the seven pools of the above-mentioned HFS model through the algorithm described above. The year of observation is 2027 and the distributions are computed over 1,000 years. The bin size b is equal to 10 ‰. The expected value and standard deviation of this distribution is 54 ± 144.

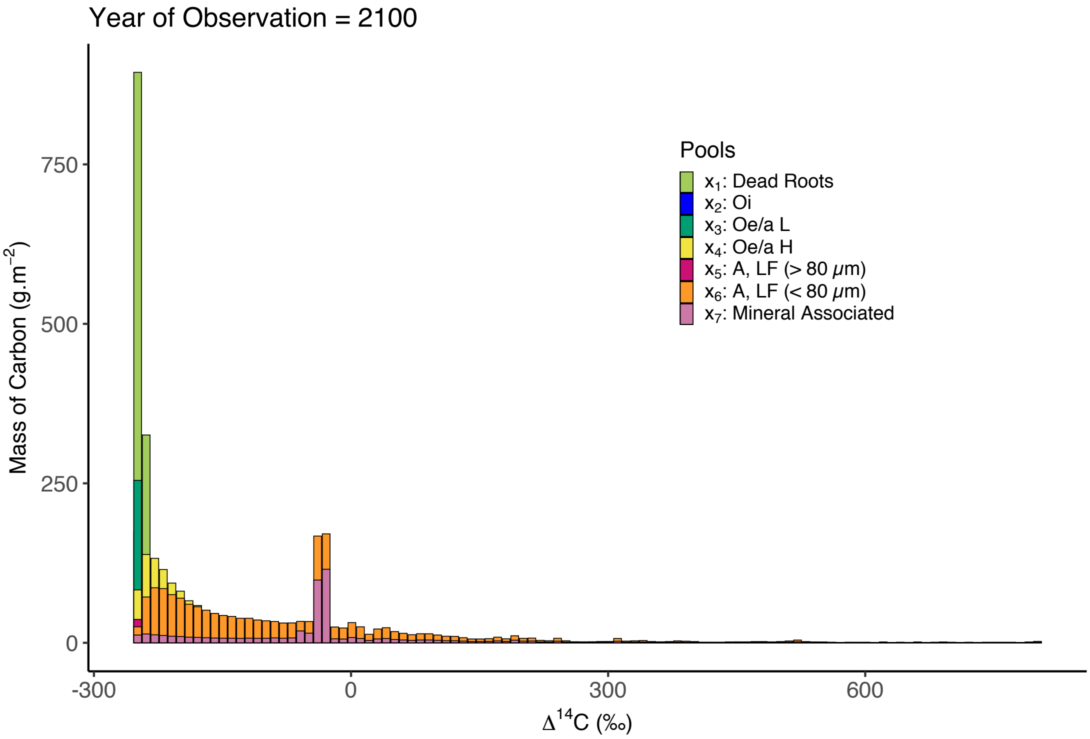

Figure 6. Δ^{14}C distributions of each of the seven pools of the above-mentioned HFS model through the algorithm described above. The year of observation is 2100 and the distributions are computed over 1,000 years. The bin size b is equal to 10 ‰. The expected value and standard deviation of this distribution is -147 ± 146.

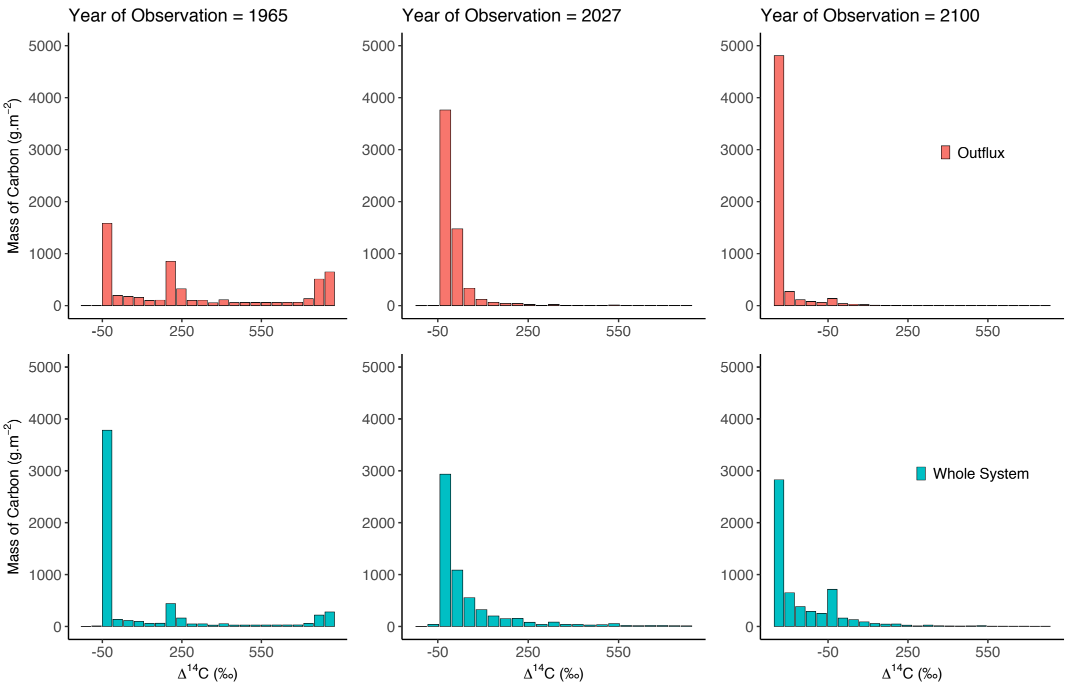

Figure 7. Δ^{14}C distributions of *Outflux* and *Whole System* of the HFS model for the years 1965, 2027 and 2100. The bin size b for all the three years is equal to 40 ‰.

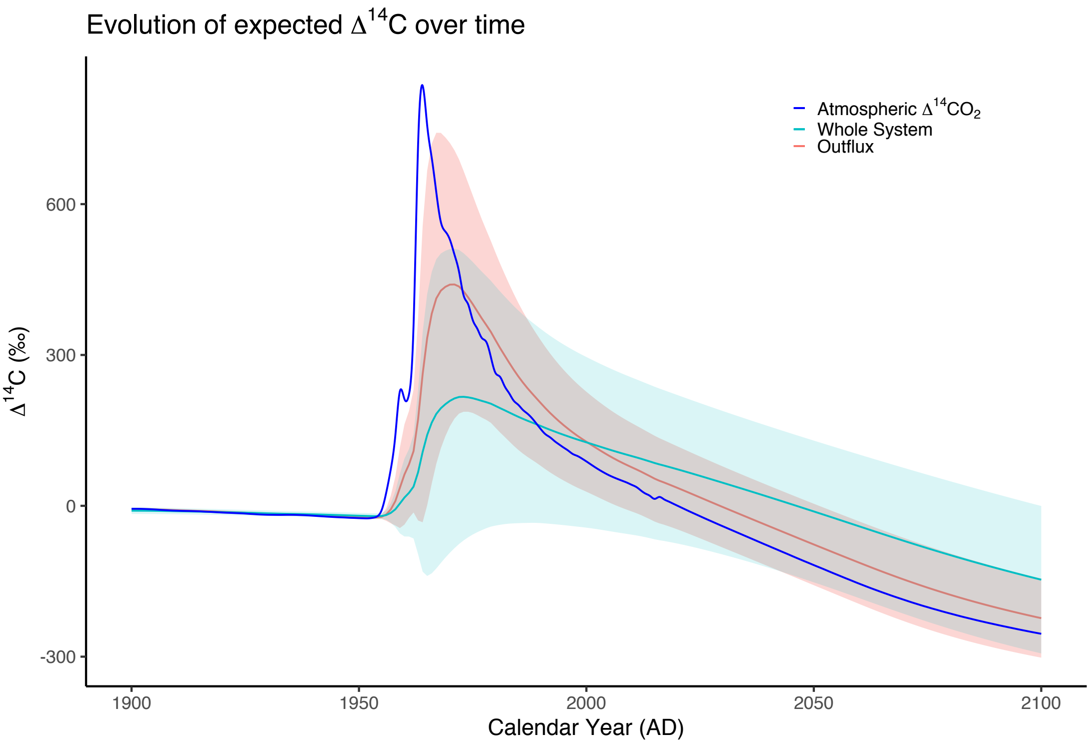

Figure 8. Evolution of the expected Δ^{14}C values of *Outflux* and *Whole System* for the HFS model between the years 1900 and 2100.

4.2 Comparison with measured data

Radiocarbon measurements of total soil CO_2 efflux at the Harvard Forest compared relatively well with the theoretical distributions of radiocarbon in the output flux obtained from our approach. Total soil CO_2 efflux includes both decomposition sources predicted by the model and root respiration, estimated by Gaudinski et al. (2000) to be $\sim 55\%$ and to have Δ^{14}C values equal to the atmosphere in any given year.

For the years 1996, 1998, 2002, and 2008, the measurements were always within the expected range (Figure 9, Table 1). In all cases, the average of the measurements was relatively close to the expected value of the theoretical distributions. However, the variability of the observations was smaller than the expected variability from the model (Figure 10).

In particular, the expected values were systematically higher in ^{14}C than average of the observations for years 1996, 1998, 2002, and 2008 by 23.5 ‰, 21.8 ‰, 15.1 ‰, and 10.8 ‰, respectively (Figure 10).

There was one order of magnitude difference between the most prominent peak and secondary peaks of the theoretical Δ^{14}C distributions. For the years 1996, 2002, and 2008, the main peak represents a mass of respired carbon within the year of $\sim 10^3$ g m^{-2}. For the year 1998, the highest peak represents a mass of respired C of $\sim 10^2$ g m^{-2}. For all those years, the bin size b was 10 ‰.

For the year 1996 (Figure 9a), the measurements of soil CO_2 efflux ranged from 104.3 ‰ to 167.3 ‰ ($\sigma = 17.3$ ‰). The theoretical most probable values also fall in this range: (112, 122]. Secondary peaks are comprised in ranges with magnitude of one bin size, starting in Δ^{14}C values of -28 ‰ and 102 ‰. For this year, our theoretical estimations also show secondary peaks in a wide range of Δ^{14}C values ranging from 122 ‰ to 212 ‰ (Table 1).

For the year 1998 (Figure 9b), the measurements of soil CO_2 efflux ranged from 66.4 ‰ to 193.9 ‰, ($\sigma = 26.2$ ‰). The main theoretical peaks are in Δ^{14}C ranges below 0 ‰ – (-37, -17] – and above 0 ‰ – (93, 153]. The peak with negative Δ^{14}C values does not appear in the soil CO_2 efflux measurements. Additionally, secondary peaks of theoretical estimations have a wide range of values, falling in the ranges: (153, 273], (323, 333], and (493, 503] in ‰ (Table 1).

For the year 2002 (Figure 9c), the measurements of soil CO_2 efflux range from 88 ‰ to 117.9 ‰, ($\sigma = 8.4$ ‰). Again, the theoretical prominent peak falls in the range: (82, 102]. One secondary peak includes the range observed in the empirical data – (102, 152]; however, additional secondary peaks of one bin size starting on -28 ‰ and 72‰ are not captured by the measurements (Table 1).

Finally, for the year 2008 (Figure 9d), the measurements of soil CO_2 efflux range from 60.8 ‰ to 104.7 ‰, ($\sigma = 13.6$ ‰). The peaks for this year are concentrated in the range (41, 121], with the highest density in the bin (51, 61] in ‰. An additional secondary peak falls in the negative part of the Δ^{14}C axis, comprising values between -29 ‰ and -19 ‰ (Table 1).

The standard deviation of the observations were 17.3 ‰, 26.2 ‰, 8.4 ‰, and 13.6 ‰ for the years 1996, 1998, 2002, and 2008, respectively, which are smaller than the expected standard deviation of the distributions, which were 107.6 ‰, 103.3 ‰, 96.3 ‰, and 89.7 ‰ for the corresponding years.

Table 1. Δ^{14}C ranges with the highest masses of radiocarbon according to our estimations; Δ^{14}C expected values according to weighted mean of mass distribution of radiocarbon; and observed Δ^{14}C mean values of soil CO_2 efflux.

	Δ^{14}C [‰]			
Year	Primary Peaks[a]	Secondary Peaks[b]	Expected value[c]	Mean value[d]
1996	(112, 122]	(-28, -18], (102, 112], (122, 212]	153 ± 107.6	129.5 ± 17.3
1998	(-37, -17], (93, 153]	(153, 273], (323, 333], (493, 503]	139.4 ± 103.3	117.6 ± 26.2
2002	(82, 102]	(-28,-18], (72, 82], (102, 152]	115.9 ± 96.3	100.8 ± 8.4
2008	(51,61]	(41, 51], (61, 121], (-29, -19]	85 ± 89.7	74.8 ± 13.6

a For 1996, 2002 and 2008, masses $\sim 10^3$ g m^{-2}; For 1998, masses $\sim 10^2$ g m^{-2};
b For 1996, 2002 and 2008, masses $\sim 10^2$ g m^{-2}; For 1998, masses ~ 10 g m^{-2};
c Expected value of theoretical radiocarbon distribution of the Outflux (weighted mean);
d Mean value of the Δ^{14}C values measured on soil CO_2 efflux from the Harvard Forest.

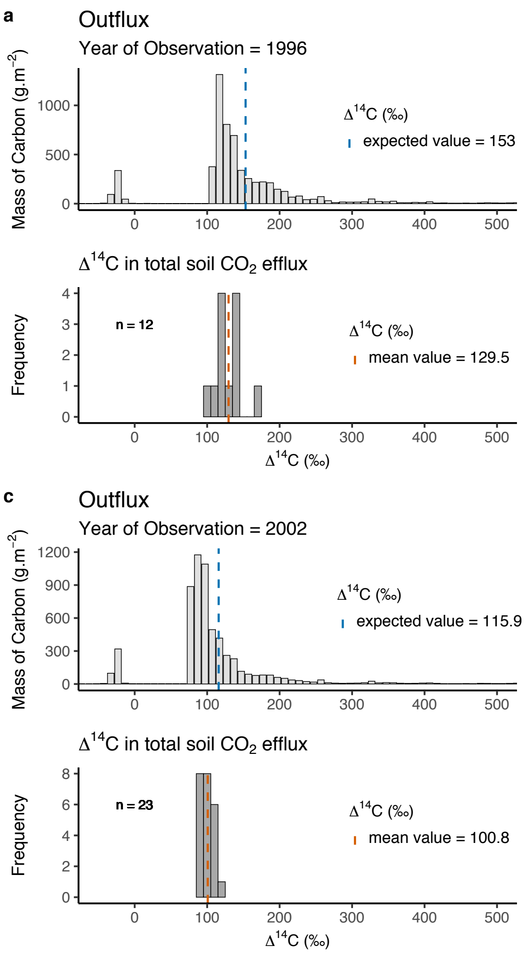

Figure 9. Comparison between theoretical radiocarbon distribution and independent empirical data. **a**: Year of observation equals to AD 1996; **b**: Year of observation equals to AD 1998; **c**: Year of observation equals to AD 2002; **d**: Year of observation equals to AD 2008.

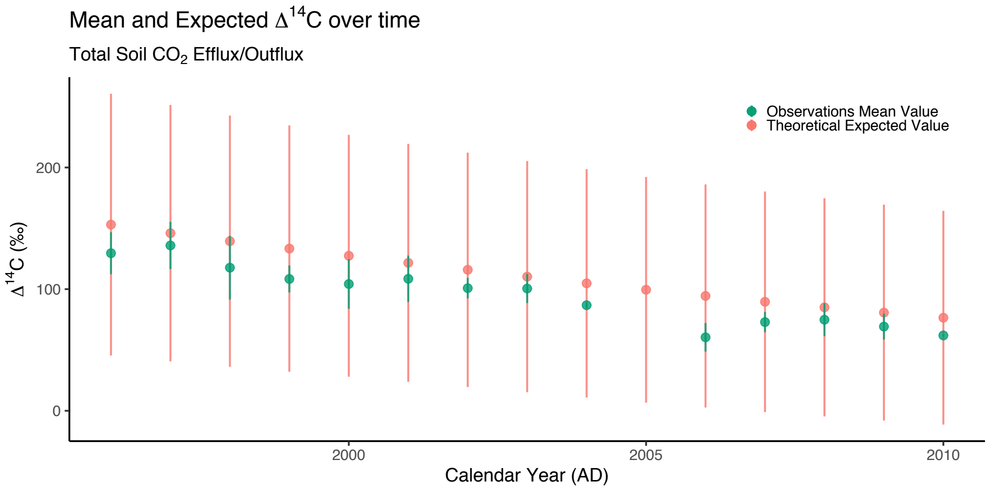

Figure 10. Change over time of the expected Δ^{14}C values and of the mean Δ^{14}C values of the total soil CO_2 efflux in the Harvard Forest (HFS model).

5 Discussion

5.1 How do distributions of radiocarbon change over time as a consequence of changes in atmospheric radiocarbon?

Our results clearly showed that distributions of radiocarbon in a compartmental system change considerably over time, despite the stationarity of the age and transit time distributions for systems at steady-state, where the total mass of carbon does not change over time. These changes reflect recent and expected dramatic changes in the isotopic signature of the inputs originating in the atmosphere, including the bomb spike and fossil fuel dilution.

For fast cycling pools, we expect changes to match that of the radiocarbon content in the atmosphere. Consequently, the radiocarbon distributions for fast cycling pools present peaks in Δ^{14}C values similar to those from the contemporary atmospheric radiocarbon. That is an effect of the fast response of highly dynamic pools to the variations in the isotopic composition of the system inputs. As fast pools are the major contributors to the output flux, the total respiration also has similar narrow distributions close to the atmospheric Δ^{14}C in the year of observation/sampling (t_0).

For slow cycling pools that receive carbon from other pools, we expect wider distributions that include contributions from C fixed decades to centuries in the past. Thus, bomb ^{14}C takes a longer time to be observed in the radiocarbon distributions.

As a consequence of fossil fuel (^{14}C-free) emissions to the atmosphere, dilution of atmospheric radiocarbon (*Suess effect*, Suess (1955)) is expected to affect future radiocarbon distributions. This further widens distributions in slow cycling pools, and causes fast cycling pools to have lower Δ^{14}C values than slow cycling pools. The Suess effect become particularly relevant in the distributions for future years, as shown in the distributions of radiocarbon based on the forecast of atmospheric Δ^{14}C values. The Δ^{14}C in the atmosphere is estimated to achieve values as low as ca. -254 ‰ in 2100 for the RCP8.5 scenario (Graven, 2015). Such low values can appear with relatively high density in two cases: (i) if the pool cycles fast but the Δ^{14}C values in the atmosphere present high dilution (as in 2100), or (ii) with natural or bomb, however non-diluted, Δ^{14}C values in the atmosphere, but in very slow cycling pools (i.e., >2,500 yrs of carbon age). The latter case reflects sufficient time for radioactive decay to reduce radiocarbon values in the carbon residing in the system. In experiments, this could result in an inability to distinguish faster and slower cycling pools using $\Delta^{14}C$ expected values. Thus one advantage of using these radiocarbon distributions is to get insight into the dynamics of transfers in the compartmental system, and to emphasize when these becomes less meaningful in the future years. Such issues can begin as soon as in 2027, when the $\Delta^{14}C$ values start to decline to values never observed before by natural processes (i.e., without the anthropogenic effects such as the fossil fuel emissions). In the forecast for central Europe (Sierra, 2018), this transition year occurs as soon as 2022. This underlines the urgency of measurements in the current situation and the use of archived samples from the last decades, to emphasize the difference between fast pools that will track the changing atmosphere and slower pools that adjust more gradually and retain bomb ^{14}C signals even in future decades.

5.2 How do empirical data compare to these conceptual radiocarbon distributions?

Measurements of radiocarbon in the output flux of a soil system, suggest that field measurements capture the mean value of the distributions, but not necessarily its variability.

Although we do not have independent observations available for specific pools to compare with our model predictions, we expect that for fast cycling pools the measurements will fall in a narrow range of $\Delta^{14}C$ values, as can be observed in experiments assessing the fossil fuel CO_2 distribution by measurements of $\Delta^{14}C$ on deciduous leaves (Santos et al., 2019). For slow cycling pools, we would expect that the variability of $\Delta^{14}C$ experimental data will be broader.

Carbon pools that cycle slowly can be very important for climate change mitigation, since they could store carbon for a longer time. Therefore, an accurate understanding of their dynamics is crucial. A valuable tool to assess these dynamics is using radiocarbon as a tracer to further constrain models. However, based on our results and interpretations, we believe that future research work should attempt at better capturing the variability of radiocarbon in such pools.

5.3 What insights can these distributions provide for experimental and sampling design for improving model-data comparisons by capturing the entire variability of $\Delta^{14}C$ values?

Overall, our results have implications for the interpretation of measured radiocarbon data and the design of empirical studies for improved understanding of carbon dynamics and comparison with models. The number of samples required to adequately represent the internal variability in radiocarbon depends on the year of observation and the particular compartment of interest. A priori determining sample sizes may be a suitable approach for future studies. For samples already collected, caution must be taken in interpreting the results, since a bulk measurement may not capture the whole distribution of possible radiocarbon values.

Our study opens up new opportunities to empirically determining radiocarbon distributions in compartmental systems. For example, this could be achieved by sampling designs that are representative of the compartments with higher variance, making sure the number of samples catches the entire potential variability. This way, it should be possible to determine empirical radiocarbon distributions.

Empirical determination of radiocarbon distributions in compartmental systems could be used to obtain age and transit time distributions using inverse statistical methods. This offers tremendous opportunities for accurate estimations of time metrics, incorporating the complexity of biological systems through multiple interconnected compartments. However, more research is still needed to determine whether radiocarbon distributions map to unique age and transit time distributions. To guarantee the uniqueness of the age and transit time distributions from compartmental systems, one should be able to assure that only one combination of rates in the compartmental matrix builds the estimated distributions.

Moreover, as pointed out by Gaudinski et al. (2000), limited information about the cycling rates are obtained by ^{14}C measurements of bulk SOM made at a single point in time. Therefore, being able to compute radiocarbon distributions for different years of observation could improve the interpretations of the time-evolution of soil radiocarbon in terms of carbon dynamics.

6 Conclusion

Compartmental models are a common approach to describe the dynamics of open systems, particularly when modeling the carbon cycle in ecosystems. The mathematical equations developed to obtain age and transit time distributions are a robust approach already used in several contexts and, therefore, using these distributions to obtain radiocarbon distributions in the same systems is a powerful method. The algorithm presented, besides being simple, demonstrated the potential power of the method. It also showed how, for a specific model, predictions can be compared with experimental data.

Radiocarbon distributions can be used together with the known changes in atmospheric $\Delta^{14}CO_2$ to evaluate how models predict the changing distributions of radiocarbon in each compartment and its output over that last decades. This provides a powerful method to test models against observations and to refine model representations of C dynamics in soils and ecosystems.

Our results also have shown that the heterogeneity of the ecosystems described through the mixing of matter in the pools, is related to the shapes of the radiocarbon distributions. As opposed to age and transit time distributions for systems in steady-state, radiocarbon distributions are expected to vary over time, strongly depending on the year of observation as a consequence of the dependence on the atmospheric ^{14}C input in the system. Thus, not only the distributions' shapes will change according to the year of observation, but also their expected values, modes, and variance.

Overall, fast cycling pools with less heterogeneity present narrow shapes for all the years of observations, whereas slower cycling pools as well as more heterogeneous compartments present wider shapes and multiple peaks of $\Delta^{14}C$ for high labelled years (e.g., 1965, when the concentrations of ^{14}C in the atmosphere were almost two times higher than the natural levels).

The theoretical distributions can be estimated for specific time points, however, that is not always feasible in experiments. That means the estimations through the algorithm have to be taken carefully when one aims to compare them to empirical data. It is also important to be aware of the radiocarbon atmospheric values used to estimate the distributions, as the variation of atmospheric $\Delta^{14}C$ can influence the shapes and mean values of the distributions. In this sense, having accurate data on the ^{14}C contents in the atmosphere is key for the determination of the radiocarbon distributions in multiple interconnected compartmental systems.

Acknowledgments
The authors would like to thank Ingeborg Levin for the meaningful comments and suggestions on this work. This work is also stimulated by the scientific research developed at the Amazon Tall Tower Observatory (ATTO), which is partly funded by the German Federal Ministry of Education and Research (grant number 01LK1602A) and the Max Planck Society.

The atmospheric $\Delta^{14}CO_2$ datasets used in this research are available through Graven (2015), Graven et al. (2017), and Reimer et al. (2020). Data on the compartmental model presented in this research, including the independent $\Delta^{14}C$ data used for comparisons with our estimations are available through Sierra, Trumbore, et al. (2012).

References

Bolin, B., & Rodhe, H. (1973). A note on the concepts of age distribution and transit time in natural reservoirs. *Tellus*, *25*(1), 58–62.

Gaudinski, J. B., Trumbore, S. E., Davidson, E. A., & Zheng, S. (2000). Soil carbon cycling in a temperate forest: radiocarbon-based estimates of residence times, sequestration rates and partitioning of fluxes. *Biogeochemistry*, *51*(1), 33–69.

Goudriaan, J. (1992). Biosphere structure, carbon sequestering potential and the atmospheric 14c carbon record. *Journal of Experimental Botany*, *43*(8), 1111–1119.

Graven, H. D. (2015). Impact of fossil fuel emissions on atmospheric radiocarbon and various applications of radiocarbon over this century. *Proceedings of the National Academy of Sciences*, *112*(31), 9542–9545.

Graven, H. D., Allison, C. E., Etheridge, D. M., Hammer, S., Keeling, R. F., Levin, I., ... others (2017). Compiled records of carbon isotopes in atmospheric co2 for historical simulations in cmip6. *Geoscientific Model Development (Online)*, *10*(12).

Hogg, A. G., Heaton, T. J., Hua, Q., Palmer, J. G., Turney, C. S., Southon, J., ... others (2020). Shcal20 southern hemisphere calibration, 0–55,000 years cal bp. *Radiocarbon*, *62*(4), 759–778.

Hogg, A. G., Hua, Q., Blackwell, P. G., Niu, M., Buck, C. E., Guilderson, T. P., ... others (2013). Shcal13 southern hemisphere calibration, 0–50,000 years cal bp. *Radiocarbon*, *55*(4), 1889–1903.

Hua, Q., Barbetti, M., & Rakowski, A. Z. (2013). Atmospheric radiocarbon for the period 1950–2010. *Radiocarbon*, *55*(4), 2059–2072.

Jacquez, J. A., & Simon, C. P. (1993). Qualitative theory of compartmental systems. *Siam Review*, *35*(1), 43–79.

Jain, A. K., Kheshgi, H. S., & Wuebbles, D. J. (1997). Is there an imbalance in the global budget of bomb-produced radiocarbon? *Journal of Geophysical Research: Atmospheres*, *102*(D1), 1327–1333.

Lawrence, C. R., Beem-Miller, J., Hoyt, A. M., Monroe, G., Sierra, C. A., Heckman, K., ... others (2020). An open source database for the synthesis of soil radiocarbon data: Israd version 1.0. *Earth System Science Data*, *12*(LLNL-JRNL-775042).

Levin, I., & Kromer, B. (1997). Twenty years of atmospheric 14 co 2 observations at schauinsland station, germany. *Radiocarbon*, *39*(2), 205–218.

Levin, I., Münnich, K., & Weiss, W. (1980). The effect of anthropogenic co 2 and 14 c sources on the distribution of 14 c in the atmosphere. *Radiocarbon*, *22*(2), 379–391.

Levin, I., Naegler, T., Kromer, B., Diehl, M., Francey, R., Gomez-Pelaez, A., ... Worthy, D. (2010). Observations and modelling of the global distribution and long-term trend of atmospheric 14co2. *Tellus B: Chemical and Physical Meteorology*, *62*(1), 26–46.

Metzler, H., & Sierra, C. A. (2017, jul). Linear autonomous compartmental models as continuous-time markov chains: Transit-time and age distributions. *Mathematical Geosciences*, *50*(1), 1–34. Retrieved from `https://doi.org/10.1007%2Fs11004-017-9690-1` doi: 10.1007/s11004-017-9690-1

Naegler, T., Ciais, P., Rodgers, K., & Levin, I. (2006). Excess radiocarbon constraints on air-sea gas exchange and the uptake of co2 by the oceans. *Geophysical Research Letters*, *33*(11).

Randerson, J., Enting, I., Schuur, E., Caldeira, K., & Fung, I. (2002). Seasonal and latitudinal variability of troposphere δ14co2: Post bomb contributions from fossil fuels, oceans, the stratosphere, and the terrestrial biosphere. *Global Biogeochemical Cycles*, *16*(4).

Rasmussen, M., Hastings, A., Smith, M. J., Agusto, F. B., Chen-Charpentier, B. M., Hoffman, F. M., … others (2016). Transit times and mean ages for nonautonomous and autonomous compartmental systems. *Journal of mathematical biology*, *73*(6-7), 1379–1398.

Reimer, P. J., Austin, W. E., Bard, E., Bayliss, A., Blackwell, P. G., Ramsey, C. B., … others (2020). The intcal20 northern hemisphere radiocarbon age calibration curve (0–55 cal kbp). *Radiocarbon*, *62*(4), 725–757.

Reimer, P. J., Bard, E., Bayliss, A., Beck, J. W., Blackwell, P. G., Ramsey, C. B., … others (2013). Intcal13 and marine13 radiocarbon age calibration curves 0–50,000 years cal bp. *Radiocarbon*, *55*(4), 1869–1887.

Santos, G. M., Oliveira, F. M., Park, J., Sena, A. C., Chiquetto, J. B., Macario, K. D., & Grainger, C. S. (2019). Assessment of the regional fossil fuel co2 distribution through δ14c patterns in ipê leaves: The case of rio de janeiro state, brazil. *City and Environment Interactions*, *1*, 100001.

Sierra, C. (2018). Forecasting atmospheric radiocarbon decline to pre-bomb values. *Radiocarbon*, *60*(4), 1055–1066.

Sierra, C., Ceballos-Núñez, V., Metzler, H., & Müller, M. (2018). Representing and understanding the carbon cycle using the theory of compartmental dynamical systems. *Journal of Advances in Modeling Earth Systems*, *10*(8), 1729–1734.

Sierra, C., Müller, M., Metzler, H., Manzoni, S., & Trumbore, S. (2017). The muddle of ages, turnover, transit, and residence times in the carbon cycle. *Global change biology*, *23*(5), 1763–1773.

Sierra, C., Müller, M., & Trumbore, S. (2014). Modeling radiocarbon dynamics in soils: Soilr version 1.1. *Geoscientific Model Development*, *7*(5), 1919–1931.

Sierra, C., Müller, M., Trumbore, S., et al. (2012). Models of soil organic matter decomposition: the soilr package, version 1.0. *Geoscientific Model Development*, *5*, 1045–1060.

Sierra, C., Trumbore, S., Davidson, E., Frey, S., Savage, K., & Hopkins, F. (2012). Predicting decadal trends and transient responses of radiocarbon storage and fluxes in a temperate forest soil. *Biogeosciences*, *9*(8), 3013–3028.

Stuiver, M., & Polach, H. A. (1977). Discussion reporting of 14 c data. *Radiocarbon*, *19*(3), 355–363.

Suess, H. E. (1955). Radiocarbon concentration in modern wood. *Science*, *122*(3166), 415–417.

Thompson, M. V., & Randerson, J. T. (1999). Impulse response functions of terrestrial carbon cycle models: method and application. *Global Change Biology*, *5*(4), 371–394.

Figure 1.

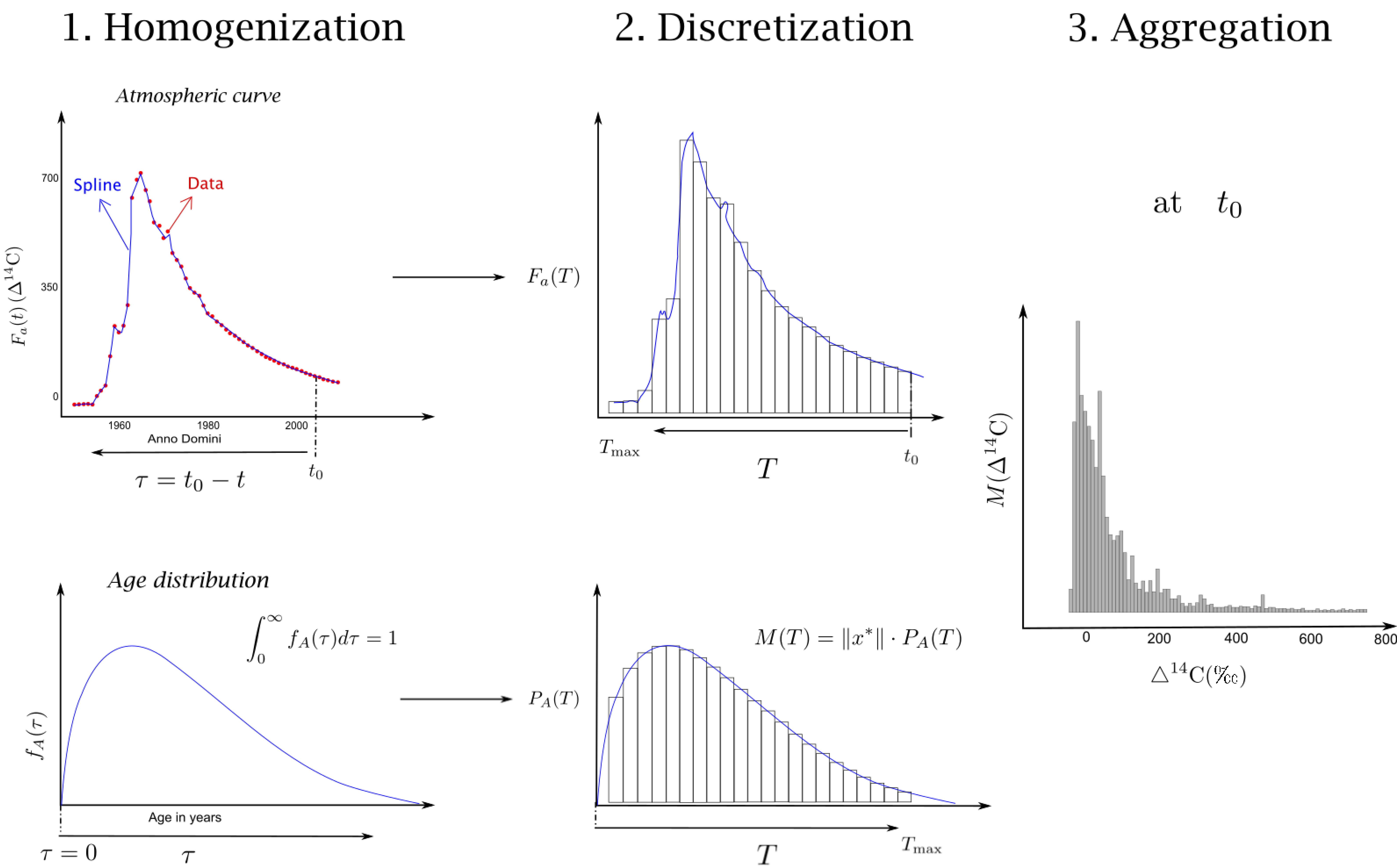

1. Homogenization
2. Discretization
3. Aggregation
Atmospheric curve
Spline
Data
700
350
0
1960
1980
2000
Anno Domini
$F_a(t)\ (\Delta^{14}C)$
$\tau = t_0 - t$
t_0
$F_a(T)$
$T_{\max}$
T
t_0
at t_0
$M(\Delta^{14}C)$
0
200
400
600
800
$\Delta^{14}C(‰)$
Age distribution
$\int_0^\infty f_A(\tau)d\tau = 1$
$f_A(\tau)$
Age in years
$\tau = 0$
τ
$P_A(T)$
$M(T) = \|x^*\| \cdot P_A(T)$
T
$T_{\max}$

Figure 2.

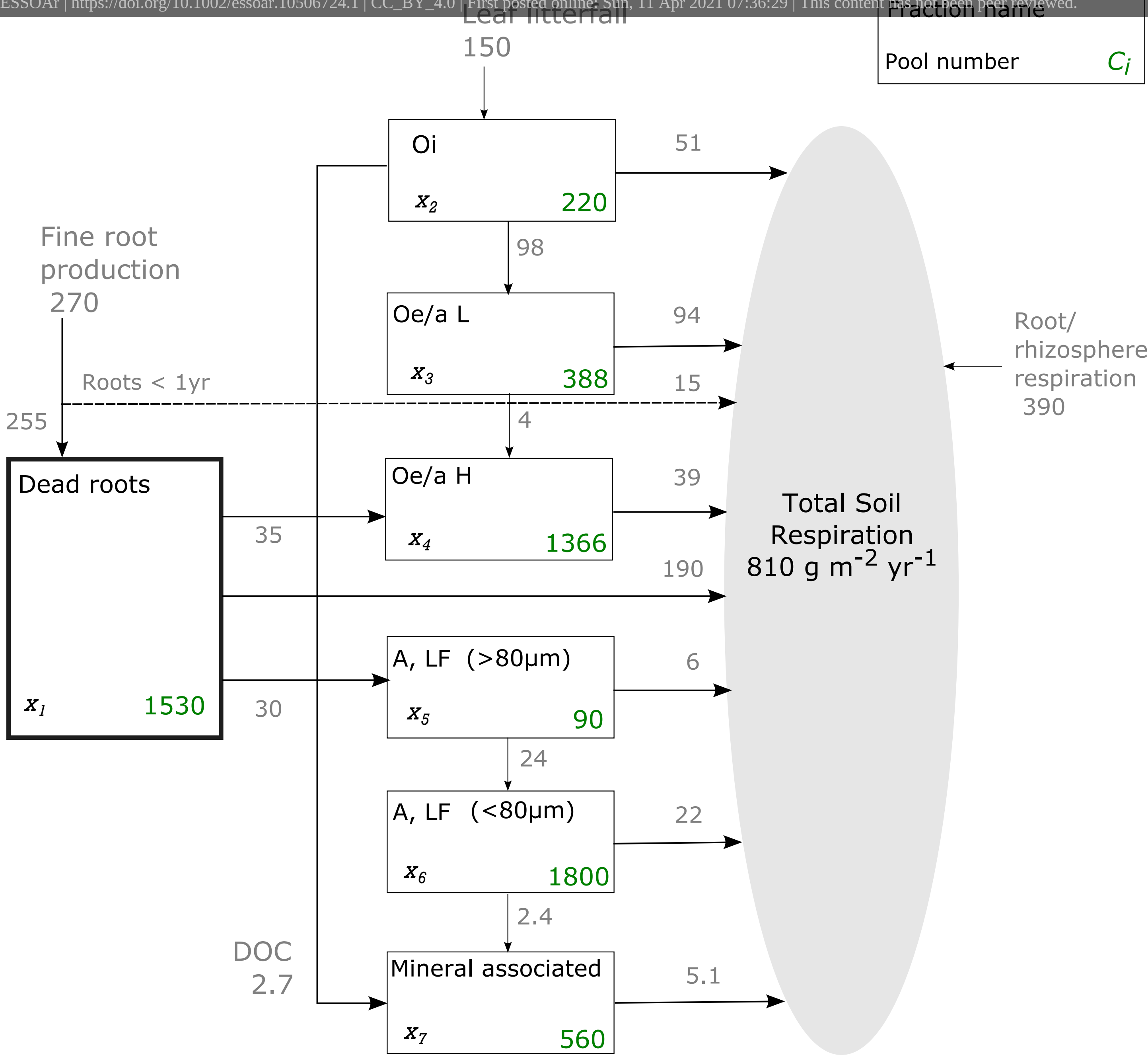

Leaf litterfall
150
Fraction name
Pool number C_i
Oi
x_2
220
51
98
Fine root production
270
Oe/a L
x_3
388
94
Roots < 1yr
15
4
255
Root/ rhizosphere respiration
390
Dead roots
x_1
1530
Oe/a H
x_4
1366
39
35
190
Total Soil Respiration
810 g m^{-2} yr^{-1}
A, LF (>80μm)
x_5
90
6
30
24
A, LF (<80μm)
x_6
1800
22
2.4
DOC
2.7
Mineral associated
x_7
560
5.1

Figure 3.

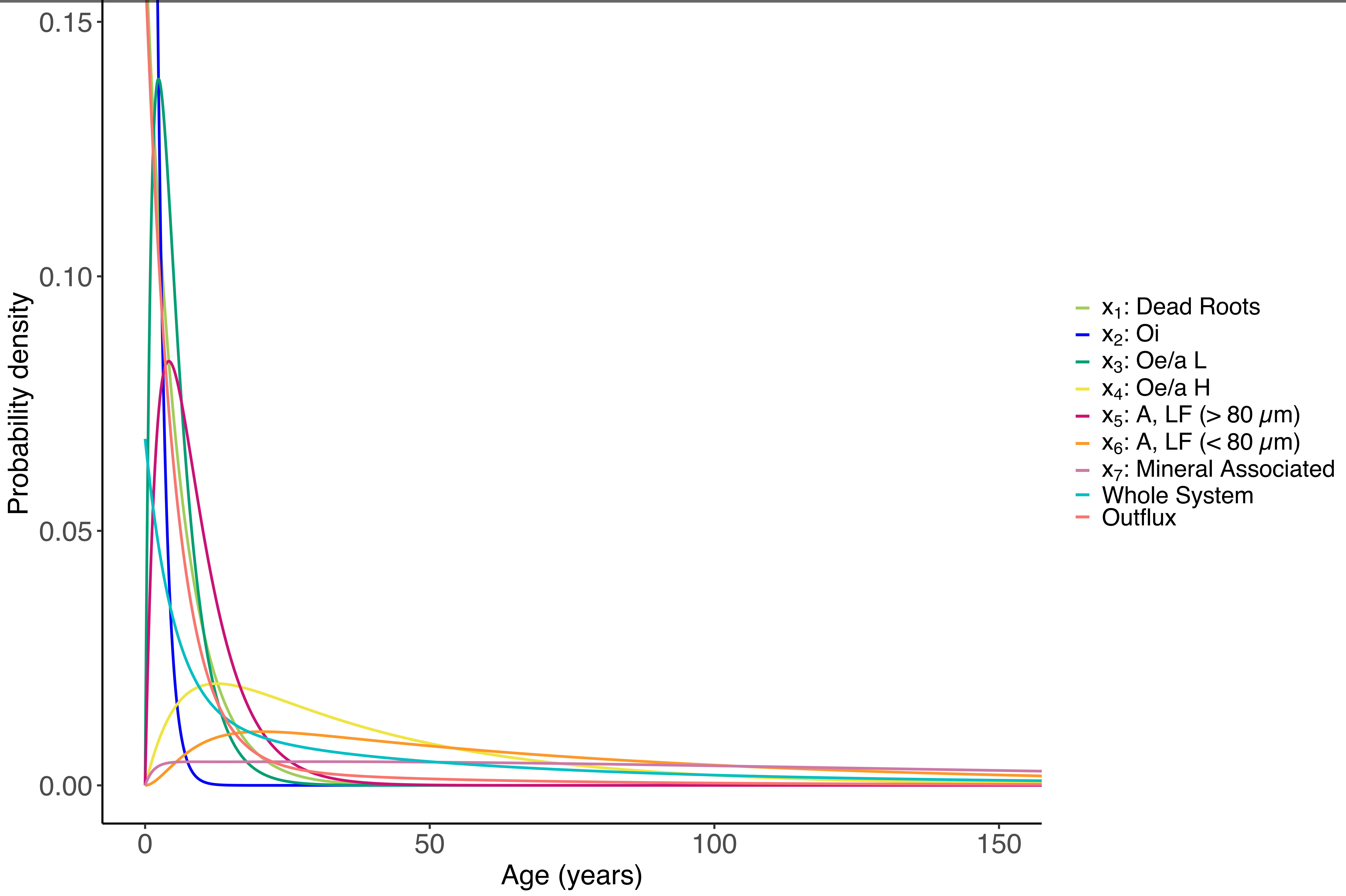

0.15
0.10
0.05
0.00
Probability density
0
50
100
150
Age (years)
x1: Dead Roots
x2: Oi
x3: Oe/a L
x4: Oe/a H
x5: A, LF (> 80 μm)
x6: A, LF (< 80 μm)
x7: Mineral Associated
Whole System
Outflux

Figure 4.

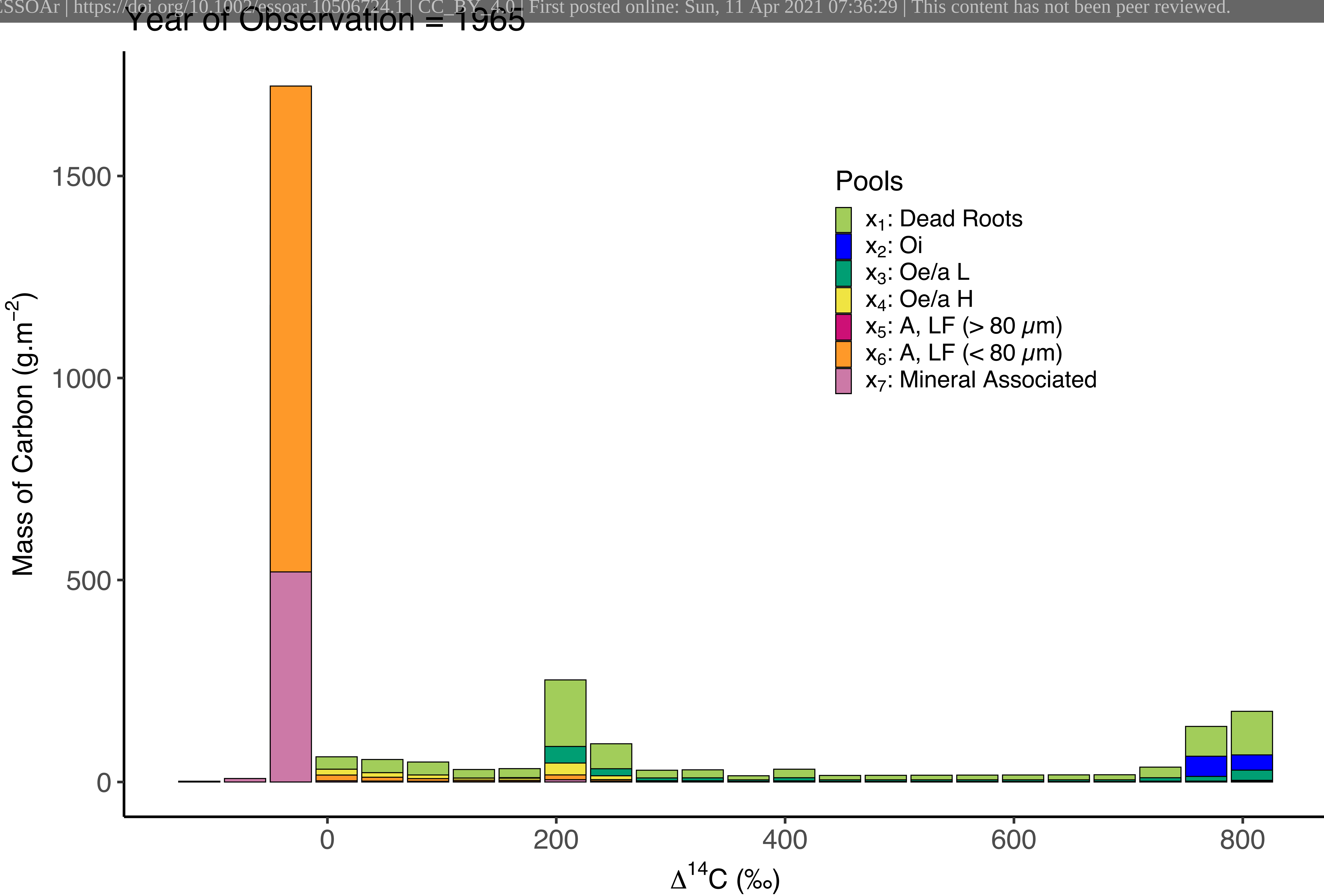
Year of Observation = 1965
Mass of Carbon (g.m^{-2})
1500
1000
500
0
0
200
400
600
800
$\Delta^{14}C$ (‰)
Pools
x_1: Dead Roots
x_2: Oi
x_3: Oe/a L
x_4: Oe/a H
x_5: A, LF (> 80 μm)
x_6: A, LF (< 80 μm)
x_7: Mineral Associated

Figure 5.

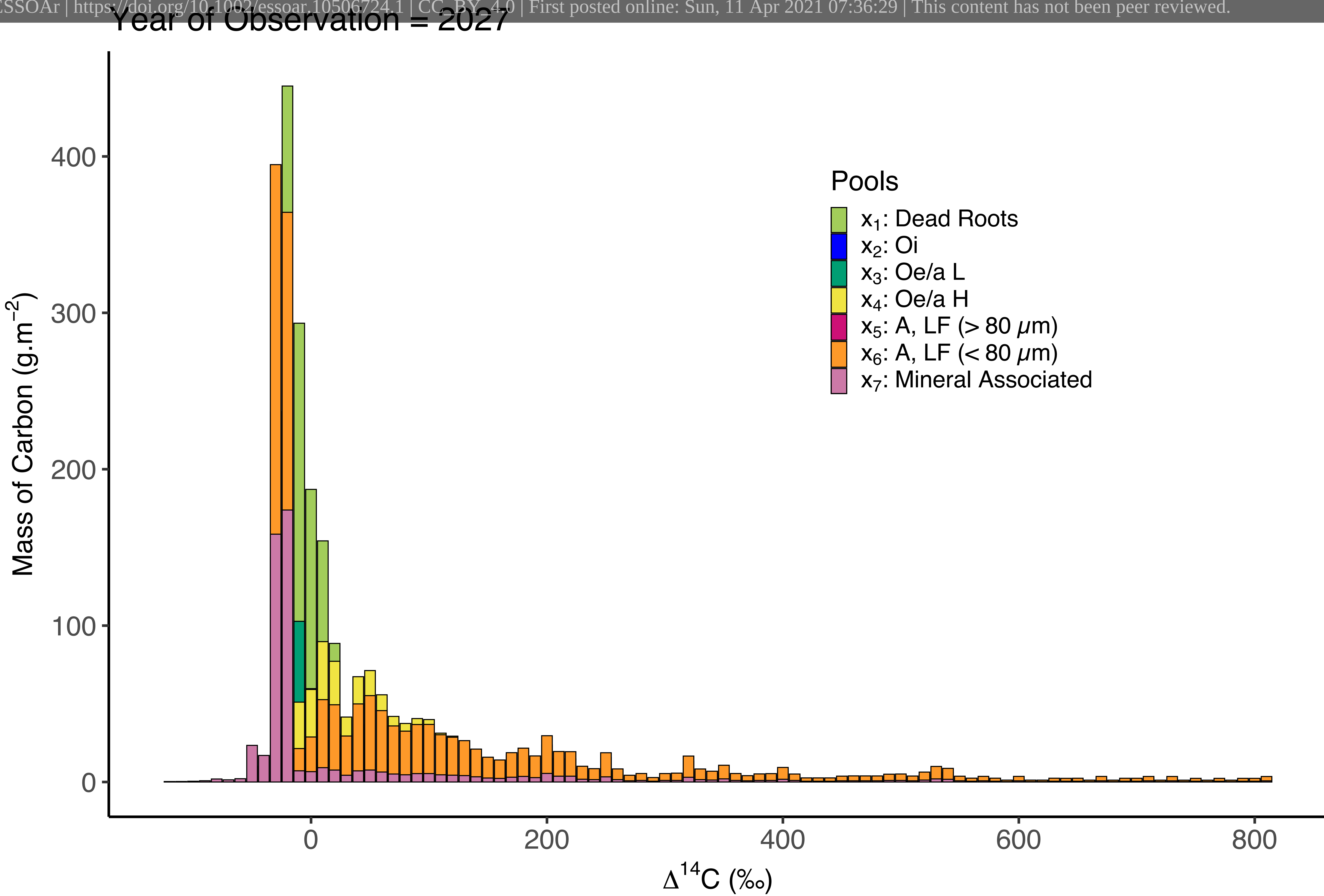
Year of Observation = 2027
Mass of Carbon (g.m⁻²)
400
300
200
100
0
Δ14C (‰)
0
200
400
600
800
Pools
x1: Dead Roots
x2: Oi
x3: Oe/a L
x4: Oe/a H
x5: A, LF (> 80 μm)
x6: A, LF (< 80 μm)
x7: Mineral Associated

Figure 6.

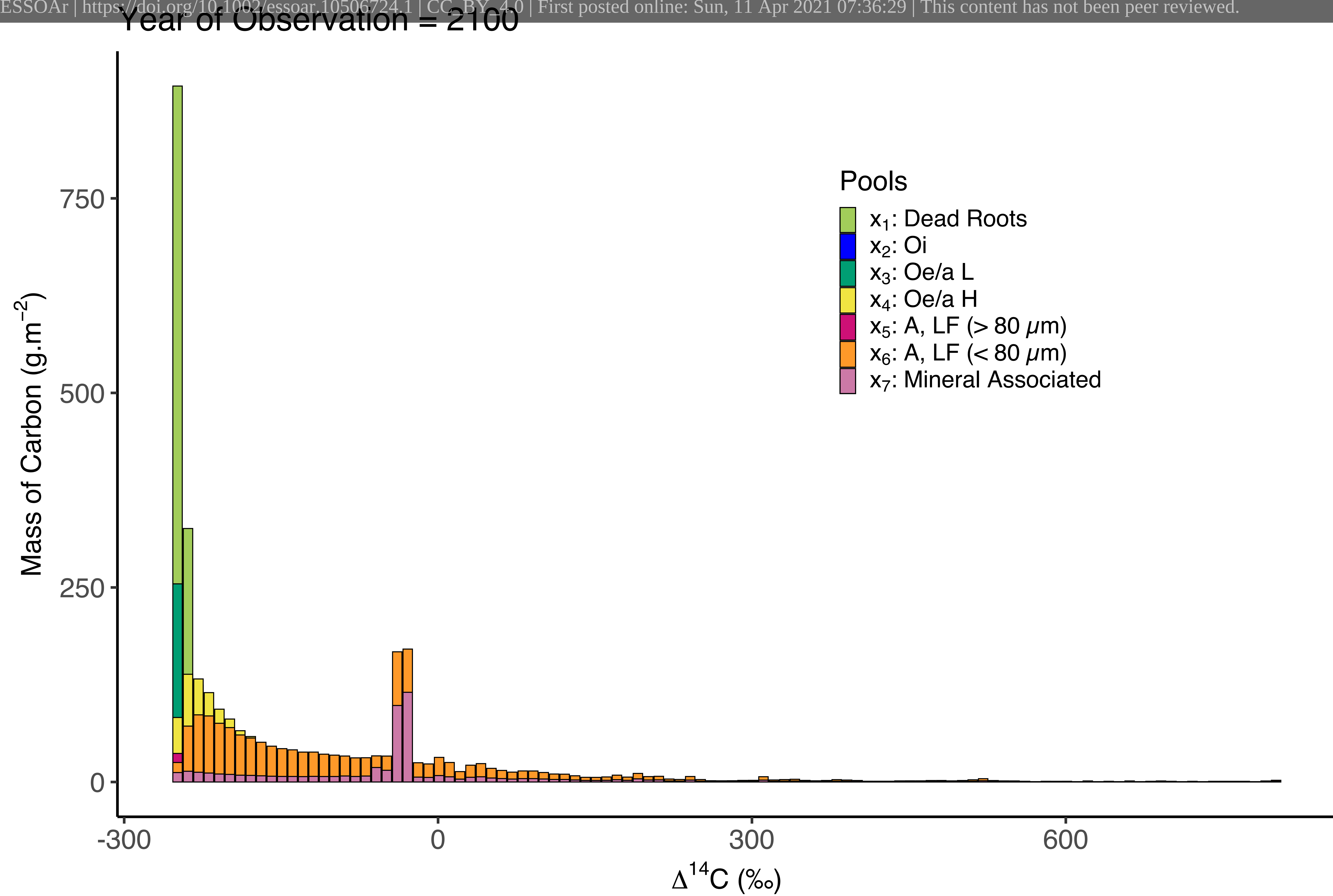

Year of Observation = 2100
Mass of Carbon (g.m−2)
750
500
250
0
-300
0
300
600
Δ14C (‰)
Pools
x1: Dead Roots
x2: Oi
x3: Oe/a L
x4: Oe/a H
x5: A, LF (> 80 μm)
x6: A, LF (< 80 μm)
x7: Mineral Associated

Figure 7.


Year of Observation = 2027
Mass of Carbon (g.m^{-2})
Outflux
Whole System
Δ^{14}C (‰)
5000
4000
3000
2000
1000
0
-50
250
550

Figure 8.

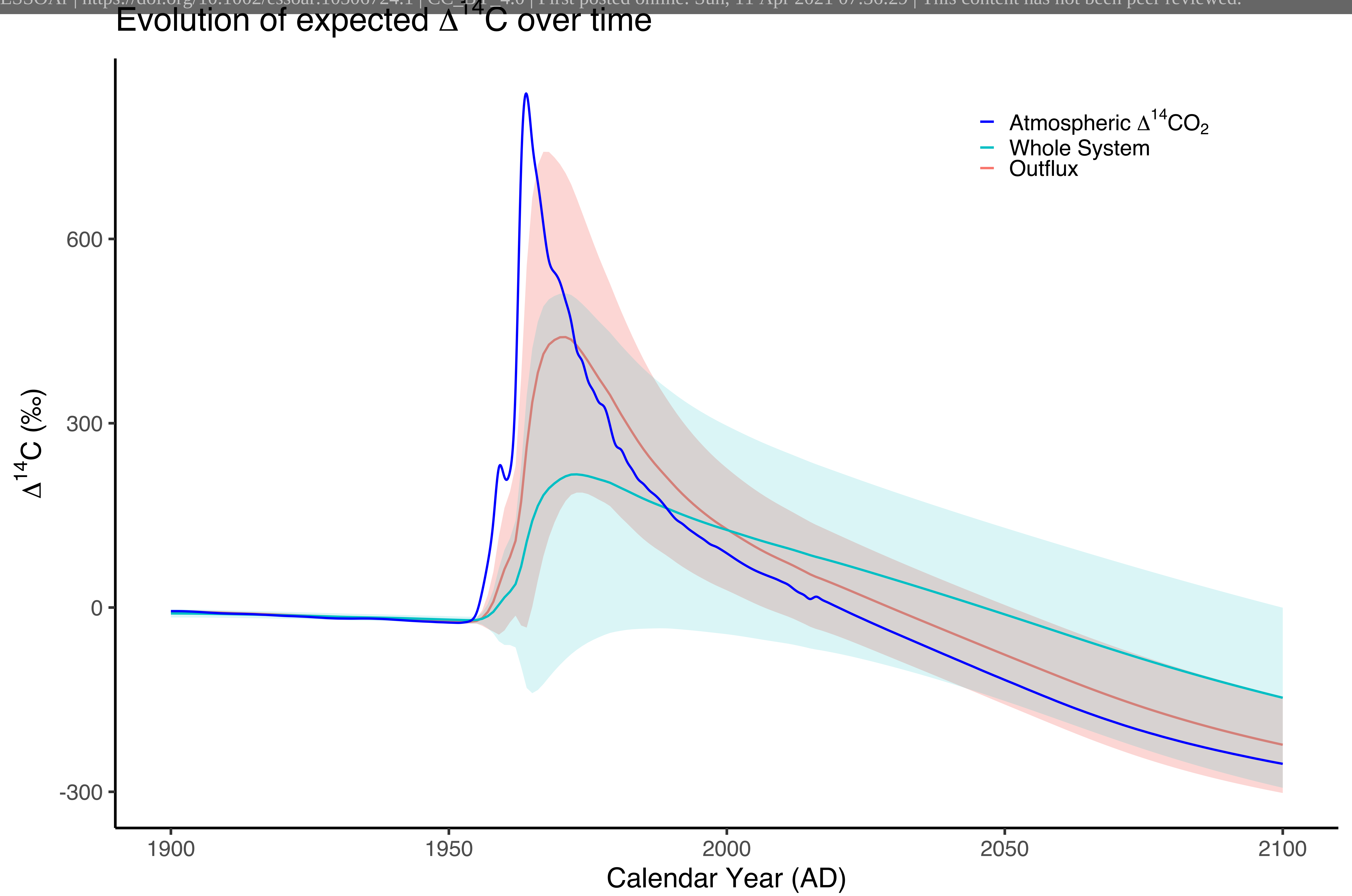
Evolution of expected Δ14C over time
Atmospheric Δ14CO2
Whole System
Outflux
600
300
0
-300
Δ14C (‰)
1900
1950
2000
2050
2100
Calendar Year (AD)

Figure 9.

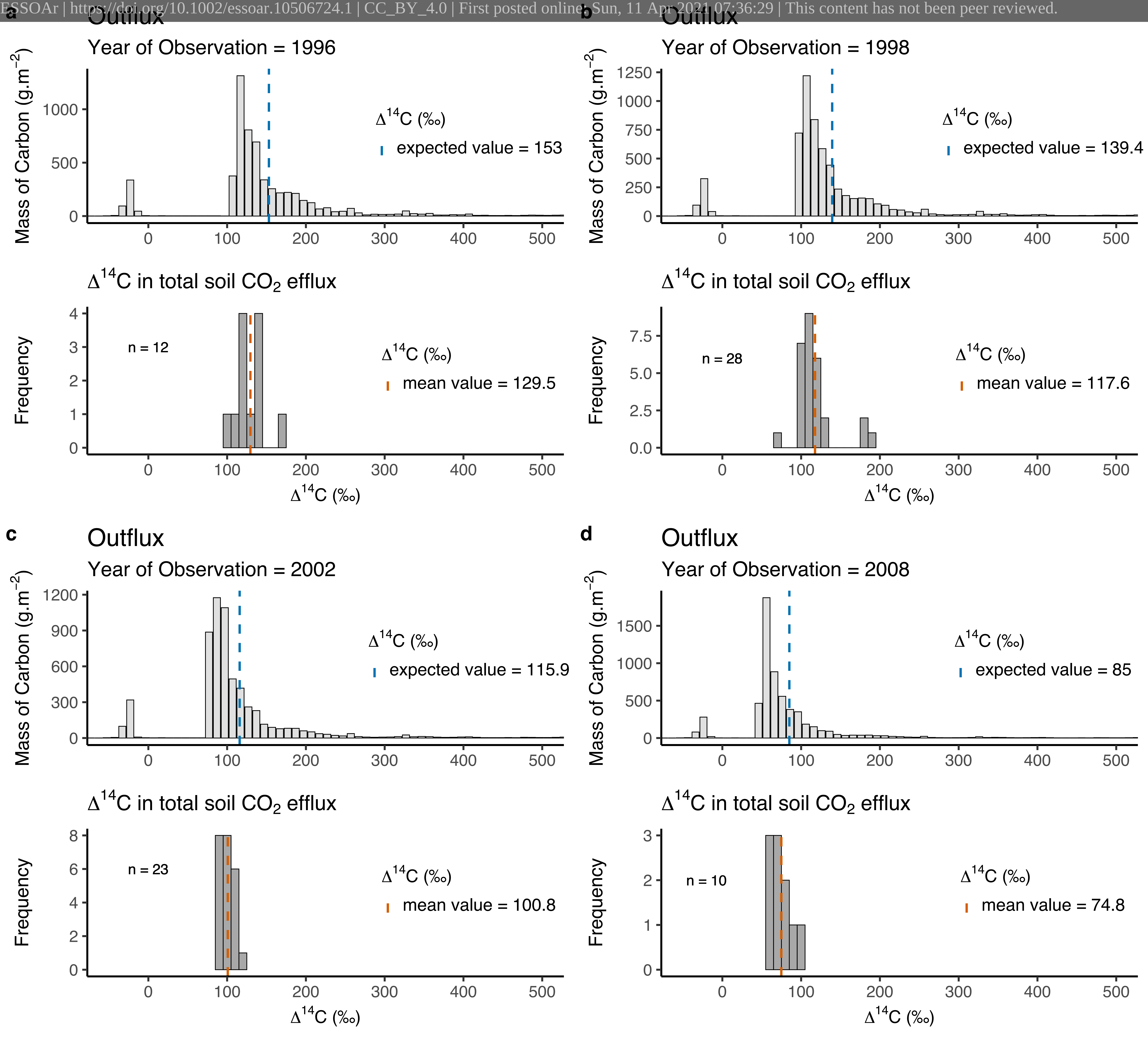
a
Outflux
Year of Observation = 1996
Mass of Carbon (g.m^{-2})
Δ^{14}C (‰)
expected value = 153
Δ^{14}C in total soil CO_2 efflux
Frequency
n = 12
mean value = 129.5
b
Outflux
Year of Observation = 1998
expected value = 139.4
n = 28
mean value = 117.6
c
Outflux
Year of Observation = 2002
expected value = 115.9
n = 23
mean value = 100.8
d
Outflux
Year of Observation = 2008
expected value = 85
n = 10
mean value = 74.8

Figure 10.

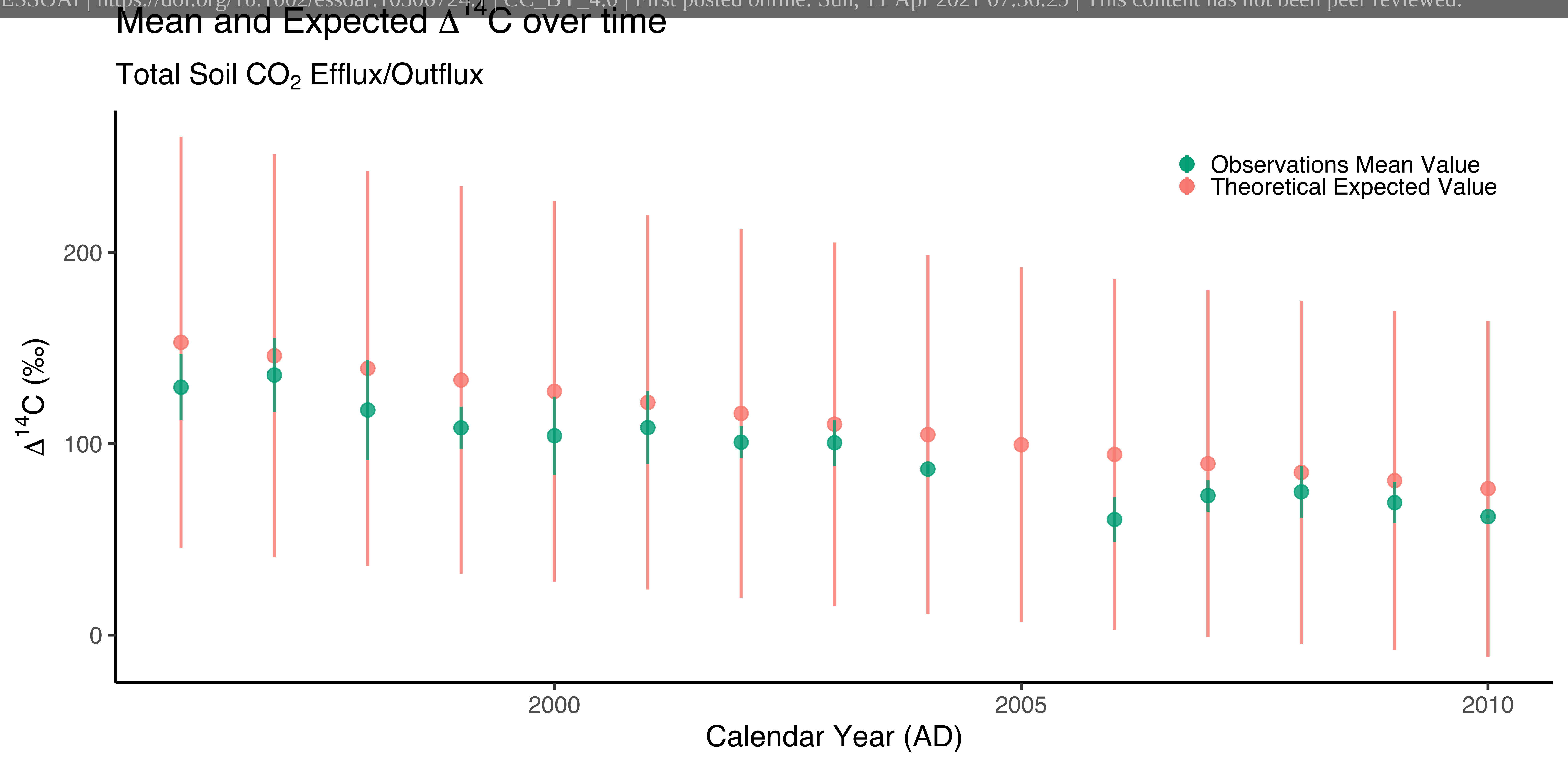
Mean and Expected Δ14C over time
Total Soil CO2 Efflux/Outflux
Observations Mean Value
Theoretical Expected Value
Δ14C (‰)
200
100
0
2000
2005
2010
Calendar Year (AD)